AD-A081 871 SYSTEMS RESEARCH LABS INC DAYTON OHIO RESEARCH APPLI--ETC F/G 21/5
MATERIAL EVALUATION. PART I. MECHANICAL PROPERTY TESTING AND MA--ETC(U)
SEP 79 N E ASHBAUGH F33615-76-C-5191
UNCLASSIFIED SRL-6909-01 AFML -TR-79-4127-PT-1 NL

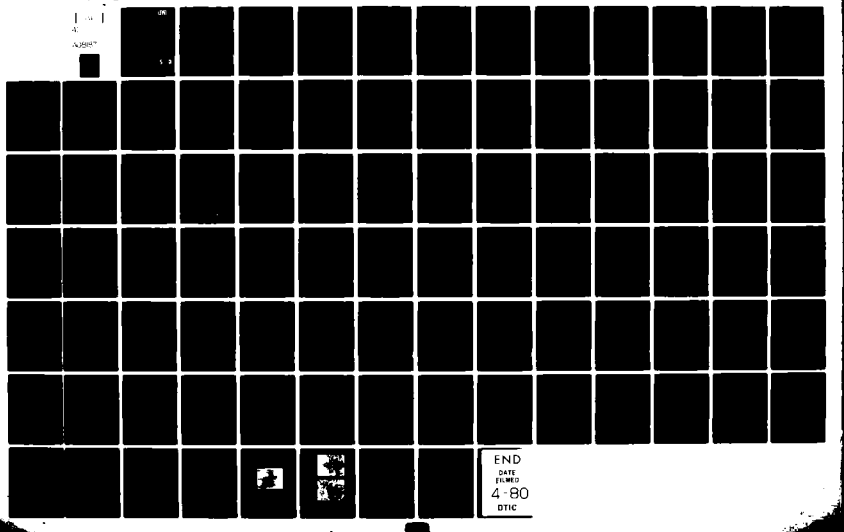

END
DATE FILMED
4-80
DTIC

AFML-TR-79-4127

Part I

# MATERIAL EVALUATION: PART I - MECHANICAL PROPERTY TESTING AND MATERIALS EVALUATION AND MODELING

N. E. Ashbaugh, Ph.D.
Research Applications Division
Systems Research Laboratories, Inc.
2800 Indian Ripple Road
Dayton, OH 45440

SEPTEMBER 1979

TECHNICAL REPORT AFML-TR-79-4127 Part I
Final Report for Period April 1976 to June 1979

Approved for public release; distribution unlimited.



AIR FORCE MATERIALS LABORATORY
AIR FORCE WRIGHT AERONAUTICAL LABORATORIES
AIR FORCE SYSTEMS COMMAND
WRIGHT-PATTERSON AIR FORCE BASE, OH 45433

*NOTICE*

*When Government drawings, specifications, or other data are used for any purpose other than in connection with a definitely related Government procurement operation, the United States Government thereby incurs no responsibility nor any obligation whatsoever; and the fact that the government may have formulated, furnished, or in any way supplied the said drawings, specifications, or other data, is not to be regarded by implication or otherwise as in any manner licensing the holder or any other person or corporation, or conveying any rights or permission to manufacture, use, or sell any patented invention that may in any way be related thereto.*

*This report has been reviewed by the Information Office (OI) and is releasable to the National Technical Information Service (NTIS). At NTIS, it will be available to the general public, including foreign nations.*

*This technical report has been reviewed and is approved for publication.*

T. Nicholas

THEODORE NICHOLAS
PROJECT ENGINEER
METALS BEHAVIOR BRANCH
METALS AND CERAMICS DIVISION

N G Tupper

NATHAN G. TUPPER, Chief
METALS BEHAVIOR BRANCH
METALS AND CERAMICS DIVISION

*"If your address has changed, if you wish to be removed from our mailing list, or if the addressee is no longer employed by your organization please notify* AFML/LLN *,W-PAFB, OH 45433 to help us maintain a current mailing list".*

*Copies of this report should not be returned unless return is required by security considerations, contractual obligations, or notice on a specific document.*

AIR FORCE/56780/25 February 1980 — 300

(19) TR-79-4127-PT-1

UNCLASSIFIED

SECURITY CLASSIFICATION OF THIS PAGE (When Data Entered)

## REPORT DOCUMENTATION PAGE

READ INSTRUCTIONS BEFORE COMPLETING FORM

(13) 1. REPORT NUMBER: AFML-TR-79-4127-Part I

2. GOVT ACCESSION NO.

(9) 3. RECIPIENT'S CATALOG NUMBER

(6) 4. TITLE (and Subtitle): Materials Evaluation, Part I, Mechanical Property Testing and Materials Evaluation and Modeling.

(14) SRL-6999-01

5. TYPE OF REPORT & PERIOD COVERED: Final Report, Apr 76—Jun 79

6. PERFORMING ORG. REPORT NUMBER: Final

(10) 7. AUTHOR(s): Noel E. Ashbaugh Ph.D.

(15) 8. CONTRACT OR GRANT NUMBER(s): F33615-76-C-5191

9. PERFORMING ORGANIZATION NAME AND ADDRESS
Systems Research Laboratories, Inc.
2800 Indian Ripple Road
Dayton, OH 45440

10. PROGRAM ELEMENT, PROJECT, TASK AREA & WORK UNIT NUMBERS
Prog. Element 62102F,
Proj. 7351, Task Area 735106
Work Unit 73510690

11. CONTROLLING OFFICE NAME AND ADDRESS
Air Force Materials Laboratory
AFML/LLN
Wright-Patterson AFB, OH 45433

(11) 12. REPORT DATE: Sep 1979

13. NUMBER OF PAGES: 89 (12) 90

14. MONITORING AGENCY NAME & ADDRESS (if different from Controlling Office)
(16) 7351
(17) 06

15. SECURITY CLASS. (of this report): UNCLASSIFIED

15a. DECLASSIFICATION/DOWNGRADING SCHEDULE

16. DISTRIBUTION STATEMENT (of this Report)

Approved for public release, distribution unlimited.

17. DISTRIBUTION STATEMENT (of the abstract entered in Block 20, if different from Report)

18. SUPPLEMENTARY NOTES

19. KEY WORDS (Continue on reverse side if necessary and identify by block number)

Fracture mechanics, fatigue-crack propagation, creep-fatigue interaction, life predictions, crack growth under spectrum loads, creep crack growth, finite-element analysis, boundary-integral equations, elevated-temperature crack-growth testing, compliance, stress-intensity factor

20. ABSTRACT (Continue on reverse side if necessary and identify by block number)

To accomplish the assessment of the characteristics of materials which are currently being used or which may be used in airframes and in gas-turbine engines, the following three tasks were performed--development and implementation of mechanical test methods, research on the application of solid mechanics to failure prediction, and investigation of environmental effects upon mechanical behavior. Some of the test methods which were developed in the first task were a low-cycle-fatigue (LCF) test capability, an experimental set-up to evaluate crack growth under sustained load, and a capability

over

DD FORM 1 JAN 73 1473 EDITION OF 1 NOV 65 IS OBSOLETE

UNCLASSIFIED

SECURITY CLASSIFICATION OF THIS PAGE (When Data Entered)

5 E

7111

to conduct crack-growth tests under spectrum loads. In these tests the temperature range was normally between 538°C (1000°F) and 760°C (1400°F), and the specimen geometries were uniform gage specimens for the LCF tests, compact-type (CT) specimens for the sustained-load crack-growth tests, and CT and wedge-opening-loaded (WOL) specimens for crack-growth tests under spectrum loads. The tests which were conducted on material behavior provided data for at least 30 reports and journal articles. These tests, in addition to the previously developed tests, included uniaxial tension and compression tests, creep tests, fatigue-life tests, and single and multiple overload and underload tests. The temperature range for these tests was between room temperature and 760°C (1400°F). Equipment and instrumentation which were designed and fabricated for these tests included resistant furnaces, induction coils, d.c. conditioners, and power controllers.

The application of solid mechanics to life and failure prediction led to the following investigations: 1) An examination and assessment of LCF models in the prediction of lifetimes for crack initiation in Ni-base superalloys, 2) An experimental and analytical investigation on the use of a precracked coupon mounted onto a dogbone specimen which simulated a structure having a crack in it; the results were analyzed to determine whether the effect of service loads on the crack growth in the structure could be monitored by the precracked coupon, 3) An analysis of the stress-intensity factors for a strip containing an eccentric crack through application of singular-integral equations and boundary integral equations; functional expressions for the stress-intensity factors were determined from a least-squares fit to the analytical results, 4) An effort in the area of finite-element analysis directed toward providing operational codes which would be employed in research investigations of crack-growth modeling and testing; codes were developed for two- and three-dimensional linear-elastic analysis of geometries having cracks, 5) Investigation of possible applications of compliance measurements at elevated temperature for automating the evaluation of crack lengths, determining an effective crack length, and evaluating a test set-up.

Details of the investigation of environmental effects (corrosion inhibitors) upon mechanical properties are described in Part II of this final technical report.

## FOREWORD

This report constitutes Part I of AFML-TR-79-4127. The work described in Part I was performed at the Metals Behavior Branch, Metals and Ceramics Division, Air Force Materials Laboratory (AFML) under Contract F33615-76-C-5191, "Mechanical Property Testing and Materials Evaluation." The contract was administered under the direction of AFML by Dr. Theodore Nicholas, AFML/LLN. The program was conducted by the Research Applications Division, Systems Research Laboratories, Inc., Dayton, OH, with Dr. Noel Ashbaugh as the Principal Investigator. Generation of data on mechanical behavior was accomplished by Messrs. Richard Klinger, James Paine, Charles Bell, George Mornhinweg, Terry Richardson, Larry Cash, Odie Blackburn, and Douglas Deaton, and Ms. Susan Wallace. The investigations of creep-fatigue interactions for Ni-base superalloys were primarily conducted by Mr. Henry Bernstein. Development of analysis techniques through the application of finite-element methods was accomplished by Dr. Jalees Ahmad. The work was performed during the period April 1976 to June 1979. Part II of this report is entitled, "Development of Corrosion Inhibitors."

TABLE OF CONTENTS

TABLE OF CONTENTS (Cont'd)

## LIST OF ILLUSTRATIONS

LIST OF TABLES

# SECTION I
# INTRODUCTION

If new materials are to be applied successfully in Air Force systems, the characteristics of these materials must be evaluated and assessed under conditions encountered in service. Also, due to the increasing costs associated with the development and acquisition of advanced systems and also with the modification and maintenance of current systems, the Air Force has placed increased emphasis upon evaluating the durability of aircraft components in the airframe and in gas-turbine engines. As a result, the Air Force Materials Laboratory (AFML) is engaged in a number of research programs with the fundamental aim being to provide a technical assessment of the characteristics of materials which are used in airframes and in gas-turbine engines.

To aid in the accomplishment of this assessment, the following three tasks were performed by SRL under a contract to the Metals and Ceramics Division of AFML:

- Development and implementation of mechanical test methods.
- Research on the application of solid mechanics to failure prediction.
- Investigation of environmental effects upon mechanical behavior.

New materials having superior mechanical properties are being developed to withstand more severe in-service conditions, for example, higher operating temperatures in aircraft engines which improve performance and operating efficiency. In order to make an accurate assessment of material behavior, the materials must be subjected to specialized and unique laboratory tests. In the first task experiments were developed to simulate--as closely as possible--the operating conditions and to generate the appropriate mechanical-property data which will provide the necessary understanding of the material

behavior. Under certain conditions tests incorporating off-the-shelf equipment and standardized testing procedures were applied to obtain the data. The assessment of the material included, but was not limited to, evaluation of the stress-strain characteristics at room and elevated temperatures, fatigue and creep behavior, ductility, fatigue crack growth, fracture toughness, etc.

The second task was undertaken primarily in support of the Air Force Damage Tolerant Design Approach and the crack-initiation concept for the assessment of durability in aircraft components. Under the Damage-Tolerance Requirements, defects must be assumed to be present in critical structural components. An acceptable component design must be based upon fatigue-crack growth of the defect to a critical size under service loads. Under the concept of crack initiation, conservative life predictions are obtained from a lower bound of fatigue-life data on smooth specimens. These predictions lead to the expensive removal and replacement of engine components. Reliable predictions of airframe and engine component lifetime depend upon both the generation of accurate crack-growth and crack-initiation data and the models which were employed in the prediction of useable life of the components.

In the third task crack-growth behavior, for static and cyclic loading conditions under corrosive media, was studied for a number of aircraft materials including steels and Al alloys. The crack growth was monitored through COD measurements on fatigue-precracked compact-tension specimens. The corrosive media included distilled $H_2O$, salt solutions, and salt solutions containing anodic and cathodic inhibitors. Further experiments were conducted on specimens treated with inhibitor-impregnated paints. Metallographs and scanning electron microscopy (SEM) were employed to examine the propagating-crack path and fracture surfaces. These data were utilized in gaining an understanding of the crack-growth mechanisms. A test chamber was installed on an MTS machine and was used to study the effects of controlled atmospheric contaminants upon mechanical properties.

To conduct these tasks it was necessary to utilize the unique and sophisticated test equipment and specialized investigative techniques available at the Metals and Ceramics Division's Mechanical Test Facility at AFML. In addition, since this program complemented other investigative AFML efforts, the program was performed on-site at AFML.

The work accomplished on these three tasks has been documented in SRL R&D Status Reports[1] and Interim Technical Reports.[2] The major results on Tasks I and II are summarized in the following two sections. In cases where papers or AFML Technical Reports have been written on the investigations in these tasks, these write-ups will be cited for the details of the effort. In cases where reports are not currently available concerning additional investigations, detailed descriptions are provided in the text. Details of accomplishments under Task III are provided in Part II of this final technical report which is entitled, "Development of Corrosion Inhibitors."

## SECTION II

## DEVELOPMENT AND IMPLEMENTATION OF MECHANICAL TEST METHODS

### 1. DEVELOPMENT OF EXPERIMENTAL METHODS

The following experimental capabilities and methods were developed to update and enhance the capability of the AFML Mechanical Test Facility and to address new testing requirements with the equipment available in the laboratory.

#### a. Low-Cycle-Fatigue Test Capability

The effects of elevated temperature and inelastic cyclic strains upon Ni-base superalloys were evaluated. The test set-up was based upon axial strain control where the reversal of strain rate occurred at either preset total-strain limits or plastic-strain limits. The anticipated operating temperatures in the range 600-800°C were produced by induction heating and were maintained within ± 2°C by a temperature controller for the duration of the test.

Three different extensometers were evaluated for measuring axial strain on a 1.27-cm (0.5-in.) gage length. These extensometers were basically clip gages with extended quartz arms which were either pushed or pulled in order to maintain contact on the uniform gage section and at the same time not damage or slip on the specimen. In addition to the low-cycle-fatigue test capability, this set-up was used to determine stress-strain behavior at elevated temperatures and--in particular--the Young's modulus.

An efficient coil design for induction heating was developed which reduces the temperature gradient in the gage section of the specimen. In order to improve the coupling between the coil and the specimen, the coil was wound in such a way that the inner diameter was smaller and the windings were within 1.27 cm (0.5 in.) of the specimen. The typical temperature gradient achieved in the specimen is shown in Table I, for either Run 1 or Run 2, which indicates uniform temperature in the gage section.

TABLE I

TEMPERATURE DISTRIBUTION OF LCF SPECIMEN

| | | Temperature (°C) | |
|---|---|---|---|
| | | Run 1 | Run 2 |
| Upper Root Radius | | 626 | 609 |
| Test Section | Upper Quarter Point | 650 | 646 |
| | Midpoint* | 649/649 | 647/647 |
| | Lower Quarter Point | 647 | 648 |
| Lower Root Radius | | 592 | 603 |

*The two temperatures at midpoint are at diametrically opposed locations.

The temperature at the control point in the root radius varied widely--by as much as 30°C--with only a couple of degrees variation in the gage section when the coil was moved slightly; such movement would occur from one set-up to another, i.e., Run 1 and then Run 2 in Table I. In order to determine the appropriate control temperature at the root radius for achieving an operating temperature in the uniform gage length, several thermocouples designed to pull against the specimen during set-up and an optical pyrometer were used in attempts to measure the operating temperature in the gage section. The technique which proved to be the most reliable was to attach thermocouple wires onto the back of a thin strip [0.318 × 0.635 × 0.005 cm (0.125 × 0.25 × 0.002 in.)] of Ni-base alloy material. The smooth side of the strip could then be pulled against the specimen in order to obtain positive contact and yet minimize the possibility of scratching the gage section and thereby initiating a crack. This strip-type thermocouple indicated a temperature 4°C lower than that indicated by thermocouples which were spot welded to the gage length. The temperature at the control thermocouple at the root radius was set to achieve a temperature from the strip thermocouple which is 4°C below the operating temperature. A PMMA chamber was fabricated and placed around the MTS frame in order to reduce air currents which would affect the temperature distribution of the specimen.

The following three extensometers were evaluated in attempts to determine which design would provide the most accurate and effective means of measuring the axial strain of the specimen:

An SRL modification of an extensometer which was supplied by MTS for LCF testing.

An extensometer (which had been used at AFML for testing 2.54-cm (1-in.) gage-length specimens.

An extensometer to facilitate the experimental set-up which was designed and built at Centro Corp.

The SRL modifications of the MTS-supplied extensometer and the set-up provisions included

1. The V-shaped end of the quartz rods were used instead of the pointed end of the rods supplied by MTS.

2. Holes were drilled through the glass rods near the V-shaped ends to permit wires to be passed through the holes and attached to springs in order to pull the extensometer rod onto the specimen. (MTS had supplied a fixture which pushed the rods but was awkward to manipulate during set-up.)

3. An adjustable rig was made to hold the springs to permit adjustment of the tension in the wires and alignment with the extensometer rods.

4. A device was incorporated into the extensometer to permit an accurate gage length to be set before initiation of the test.

5. Another device was built to permit adjustment of the vertical and horizontal positioning of the coil to achieve the correct temperature profile on the specimen.

In the test set-up the load train is a combination of specimen with buttonhead adaptors attached, buttonhead grips, self-aligning hydraulic grips, the rod to the load cell, and the hydraulically actuated ram. In order to evaluate the alignment of the load train, four strain gages were spaced equally around the midsection of an LCF specimen. The strain in this specimen, when loaded in tension and compression, provided a means of determining looseness in the loading fixtures when zero load is passed through and potential eccentricity in the load train as well as a check on the strain measured by an extensometer. In typical results for the

strain-gaged specimen, irregularities in the strains were produced when the load passed through zero. An expected percent bending strain from these results for this complex load train as determined by a proposed ASTM test method* was 5%.

In concluding the evaluation of the extensometer, an LCF specimen of AF115 material having a 0.635-cm (1/4-in.) diam. and a 1.9-cm (3/4-in.) gage length was tested to determine the modulus which would be compared to the values of modulus obtained from an independent source.

Load-versus-strain curves were obtained for the following test temperatures: room temperature, 538°C (1000°F), 649°C (1200°F), 704°C (1300°F), and 760°C (1400°F). The elevated temperatures were produced by induction heating. The tests were conducted in load control, ramp through zero, with maximum and minimum loads of ± 1000, ± 2500, and ± 4000 lb. The time required for a complete loading cycle was 3 sec. Thermal expansion of the material was calculated for each temperature increment. The results of these tests for the SRL-modified extensometer and the long-armed extensometer which was available at AFML are indicated in Tables II and III, respectively. Spurious operating characteristics which developed in the Centro extensometer prevented the taking of data.

In conclusion the MTS extensometer modified by SRL provided the best operational characteristics. The second extensometer having a mechanical hinge on the arms was also acceptable but was more difficult to set up than the previous extensometer. When the extensometer designed and built by the Centro Corp. was evaluated, large hysterises loops occurred in the stress-strain behavior. Since the specimen behaved elastically under the test conditions, the hysterises loops were attributed to the design of the extensometer. For use of this extensometer, extensive redesign and modifications would be required.

---

*"Sharp-Notch Tension Testing of Thick High-Strength Aluminum and Magnesium Alloy Products with Cylindrical Specimens."

TABLE II

MODULUS VALUES FOR AF115 USING SRL-MODIFIED EXTENSOMETER

| Temp (°C) | Area* ($in.^2$) | ΔP (lb.) | E ($10^6$ psi) | E+ Ref. ($10^6$ psi) |
|---|---|---|---|---|
| Room Temp. | 0.04822 | 1500 | 33.0 | 33.6 |
| 538 (1000°F) | 0.04890 | 2000 | 28.7 | 30.3 |
| | | 5000 | 29.0 | |
| | | 8000 | 28.8 | |
| 649 (1200) | 0.04909 | 2000 | 27.6 | 28.9 |
| | | 5000 | 27.4 | |
| | | 8000 | 27.2 | |
| 704 (1300) | 0.04918 | 2000 | 26.6 | 27.9 |
| | | 5000 | 26.7 | |
| | | 8000 | 26.4 | |
| 760 (1400) | 0.04928 | 2000 | 25.7 | 27.3 |
| | | 5000 | 25.6 | |
| | | 8000 | 25.6 | |

*Corrected for temperature.

+Data obtained from tests done at Mar-Test Corporation in Cincinnati, OH.

## TABLE III

## MODULUS VALUES FOR AF115 USING LONG-ARMED EXTENSOMETER

| Temp (°C) | Area* ($in^2$) | ΔP (lb.) | E ($10^6$ psi) | E+ Ref. ($10^6$ psi) |
|---|---|---|---|---|
| Room Temp | 0.04838 | 1500 | 32.8 | 33.6 |
| 538 (1000°F) | 0.04904 | 2000 | 30.2 | 30.3 |
| | | 5035 | 29.9 | |
| | | 8000 | 29.3 | |
| 649 (1200) | 0.04920 | 2000 | 28.9 | 28.9 |
| | | | 29.0 | |
| | | 5040 | 28.5 | |
| | | | 28.6 | |
| | | 8040 | 28.4 | |
| 704 (1300) | 0.04930 | 2000 | 28.2 | 27.9 |
| | | 5090 | 28.0 | |
| | | 8050 | 28.0 | |
| 760 (1400) | 0.04940 | 1990 | 27.2 | 27.3 |
| | | 5070 | 26.8 | |
| | | 8050 | 26.8 | |

*Corrected for temperature.

+Data obtained from tests done at Mar-Test Corporation in Cincinnati, OH.

b. Test Capability for Crack Growth Under Sustained Load

A furnace designed for compact-tension specimens was installed in Swedish Creep Frame 2. The furnace required a temperature controller for each side of its windings. The existing control circuits for Swedish Frames 1 and 2 were redesigned to provide an on-off control function between variable minimum and maximum current levels. A temperature-distribution determination was made at 732°C (1350°F) on a 1.27-cm-(1/2-in.)-thick compact-tension specimen of IN-100 instrumented with six thermocouples on each side and located so as to provide temperature data from top to bottom and from front to rear of the specimen. The best distribution found was ± 3°C (± 5°F) above and below the crack path and along its length. A 24-hr temperature-stability test at 732°C (1350°F) produced a variation of ± 2°C (± 4°F).

Due to the special data requirements of the test, measurement of load-line deflection throughout the test was necessary. In tests at room temperature, a common method of measuring load-line displacement involves placing a clip gage between two knife edges which has been machined on the notch surfaces to coincide with the load-line of a CT specimen. Due to the elevated temperatures of this test, clip gages could not be used. An analysis using boundary integral equations[3] indicated that measurement of the displacement between points which lie along the load-line on the top and bottom surfaces of the CT specimen provides equivalent measures of the load-line displacement. In order to measure displacements at these points, two E-shaped plates of steel were fabricated which could be attached to the points on the top and bottom of the specimen and would fit around the clevises holding the specimen. On the outside arms of these E-plates, small cones were attached to coincide with the load line. Concentric rods were suspended from these cones on each side of the specimen. The outer and inner rods on each side were attached to the body and the core of an LVDT, respectively. The LVDT's were located outside the hot zone of the furnace.

In order to confirm the results of the analysis and to make a preliminary check of the set-up, the correspondence between load-line deflection measured by a conventional clip gage and that measured by the LVDT's was determined on a 1.27-cm-(1/2-in.)-thick compact specimen of 304 stainless steel. The specimen was mounted in the Swedish creep frame; increasing loads were applied; and deflection readings were taken for the clip gage and the LVDT's. The determinations of compliance obtained from the slope of the linear portion of the load-line deflection versus load curves were made for nominal crack lengths of 1.78, 2.54, and 3.56 cm (0.7, 1, and 1.4 in.). The precracked $K_{max}$ levels were 18 ksi $\sqrt{in.}$ for the 0.7-in. crack length and 19 ksi $\sqrt{in.}$ for the 2.54- and 3.56-cm (1.0- and 1.4-in.) crack lengths.

After examination of the fracture surface, it was apparent that crack growth had occurred during the loading-unloading compliance evaluations. The surface and center crack-length measurements were taken for the narrow band that formed at the nominal crack lengths during compliance evaluations. These crack lengths and compliance values are given in Table IV. The compliance value represents an average of several measurements which varied from the average by no more than ± 3%. The predicted crack lengths from the analysis are given in Table IV for the compliance associated with displacements between the notch surfaces (clip gage) and between the top and bottom surfaces (LVDT).

Based upon the initial tests, the following test procedure to determine crack growth under sustained load was adopted:

1. Fatigue crack the specimen at room temperature to a crack length of ~ 1.63 cm (0.65 in.) at K which is less than 50% of the initial K value to be used in the test.

2. Place center punch marks 0.635 cm (1/4 in.) above crack path at 0.635-cm (1/4-in.) intervals.

3. Measure, in tool-makers microscope, the distance from the edges of the specimen to its holes, notch bottom, crack tip, and punch marks on both sides of the specimen.

TABLE IV

EXPERIMENTAL CALIBRATION AND COMPARISON WITH ANALYTICAL RESULTS FOR COMPLIANCE OF CT SPECIMEN

| Crack Lengths (surface) $\bar{a}_s$ (in.) | Crack Lengths (center) $a_c$ (in.) | Nondimensional Compliance EBC* (-) Clip Gage | Nondimensional Compliance EBC* (-) LVDT | Predicted Crack Length $a_p$ (in.) Clip Gage | Predicted Crack Length $a_p$ (in.) LVDT |
|---|---|---|---|---|---|
| 0.694 | 0.794 | 21.4 | 22.8 | 0.772 | 0.750 |
| 0.765 | 0.838 | | | | |
| 0.998 | 1.080 | 41.6 | 41.9 | 1.044 | 1.020 |
| 1.072 | 1.140 | | | | |
| 1.368 | 1.415 | 142 | 144 | 1.436 | 1.434 |
| 1.397 | 1.445 | | | | |

*For 304 stainless steel, Young's modulus $E = 29 \times 10^6$ psi and the thickness B = 0.5 in.

4. Attach and align E-plates on top and bottom of the specimen to provide pivot points for mounting the rods moving the load-line deflections from the furnace to the LVDT's located about 63.5 cm (25 in.) below the specimen and out of the hot zone.

5. Weld a thermocouple to each side of the specimen about 1.27 cm (1/2 in.) below the crack path and 1.27 cm (1/2 in.) beyond the tip of the crack.

6. Mount the specimen in the creep frame using good alignment procedures, and connect thermocouples and LVDT's.

7. Determine compliance of specimen at room temperature by recording deflections from LVDT's for a minimum of five increments of loading (and unloading), the total of which should not exceed 35% of the total test load.

8. Heat specimen to test temperature and hold for one-half hour.

9. Determine elevated-temperature compliance as in 7.

10. Apply full test load, recording load-line deflection during loading and then load-line deflection versus time at constant load. At 5-min. intervals record surface crack length to nearest 0.0025 cm (1/1000 in.) with traveling microscope at each side of the specimen or with camera on one side of specimen. Punch LVDT data onto paper tape.

11. At one-half hour intervals, determine compliance by unloading-loading as in 7.

12. Stop test by unloading when crack growth is near expected critical crack length.

13. Determine compliance as in 7.

14. Cool specimen to room temperature with small stabilizing load on creep-frame pan.

15. Determine room-temperature compliance as in 7.

16. Pull specimen apart after removing instrumentation.

17. Measure precrack and final test crack lengths from fracture surface in tool-makers microscope.

This procedure provided acceptable experimental results, with emphasis upon determining the effective crack length from compliance evaluations.

Since future tests were expected to extend beyond an 8-hr working day, photographs of the crack-tip region were taken in order to determine whether adequate surface-crack-length measurements could be made. After several trials with various lighting arrangements, focal lengths, and exposure times, it was determined that crack lengths could be measured from the photographs which were taken manually. However, due to the limiting combination of exposure time necessary to obtain clear photos and the automatic drive mechanism of the camera, it was determined that the photographic system currently available in the laboratory was not adequate to provide an automated technique for determining crack lengths.

c. Spectrum-Load Test Capability

A system composed of a Tektronix 4051/U.S. Data Systems Control Unit (SCU)[4] was purchased by AFML to provide the capability of generating a random voltage output which could be used as a load signal for an MTS test frame. However, a program had to be written if the system was to provide the output needed to simulate a load-time history which an aircraft engine component may experience in flight and to repeat the load-time history. The bulk of

the program which is given in Table V was written by SRL personnel, with a Government employee and a U.S. Data representative working out an effective means for inputting the calculated end points of the spectrum into the SCU. Final debugging of the input phase to the SCU in order to obtain a workable program was performed by SRL personnel.

Basically the program subdivides the time axis of a load spectrum into segments of constant time and computes the end points, i.e., load level, for each successive time segment to insure that the end points will follow the specified load spectrum. The signal to the MTS test frame is a ramp function which connects the end points of each segment; the best reproduction of the load spectrum is achieved when the maximum length of the time segment is the minimum of the times in the load spectrum between a maximum and a minimum load value or a minimum and a maximum load value. Since the SCU is limited to 750 end points, the current maximum time of a spectrum is equal to the constant time segment times 750.

d. Feasibility of a.c. Electric Potential System

An attempt was made to evaluate an a.c. electrical-resistance crack-length-measurement system with existing components. The a.c. signal was obtained from a PAR Model 124 lock-in-amplifier fed into a Model 2250MB electronics power amplifier and then applied at about 1-amp current level across the notched end of a CT specimen. The voltage output which should be related to crack length taken from across the notch of the specimen is sent back into the lock-in amplifier where the signal is refined and rectified to a d.c. output. The method was applied to a CT 1.27-cm- (0.5-in.-) thick specimen without success. It was also applied to a 0.03-cm- (0.01-in.-) thick specimen of a high nickel-chromium alloy. In this case the equipment appeared to respond in an acceptable manner, giving an easily measured signal with a linear relation to large crack-length changes. This demonstrated the feasibility of the method for those cases where large resistance was present, and the change in resistance with crack-length change was within the capacity of the equipment.

TABLE V

PROGRAM FOR REPEATED SPECTRUM LOADING

Listing made on 28 June 1979

```
LIST
1 [illegible] TO 100
4 [illegible] TO 2470
6 [illegible] TO 2830
1[illegible] TO 2860
1[illegible] TO 2890
[illegible] TO 2920
[illegible] TO 2940
[illegible] TO 3010
1[illegible] INIT
1[illegible] PAGE
1[illegible] PRINT "PROGRAM NOW INITIALIZED"
1[illegible] A3=0.148
1[illegible] S=0.973
1[illegible] M=2
1[illegible] R=0.1
1[illegible] N2=0
1[illegible] C=1
1[illegible] PRINT "WHAT IS THE INITIAL CRACK LENGTH?"
1[illegible] INPUT A1
1[illegible] PRINT "WHAT IS THE NOTCH LENGTH?"
1[illegible] INPUT A0
195 DIM E(300)
197 DIM S(300)
200 FOR L=1 TO 300
210 E(L)=0
220 S(L)=0
230 NEXT L
251 E(1)=A1+A0
252 S(1)=0
260 J9=1
270 ON SRQ THEN 2170
280 ON EOF (0) THEN 1540
290 SET KEY
300 I=0
```

TABLE V (Cont'd)

```
[illegible] PRINT "DO YOU KNOW WHAT K IS? IF SO ENTER ITS VALUE."
[illegible] PRINT "IF NOT, ENTER 0."
[illegible] INPUT K
[illegible] PRINT "DO YOU KNOW WHAT P IS? IF SO ENTER ITS VALUE."
[illegible] PRINT "IF NOT, ENTER 0."
[illegible] INPUT C
[illegible] PRINT "ENTER EQUATION NUMBER; (1 OR 2)"
[illegible] INPUT X
[illegible] IF K=0 THEN 530
400 REM *** CALCULATE PMIN. & PMAX.
[illegible] PAGE
[illegible] I=I+1
[illegible] IF X=2 THEN 480
440 REM *** USE EQN. #1
[illegible] GOSUB 1960
[illegible] L1=K*B*SQR(W)/Y
470 GO TO 510
480 REM *** USE EQN. #2
490 GOSUB 2080
500 L1=K*B*W/Y*SQR(A)
510 L1=INT(L1*1000)
520 GO TO 700
530 REM *** CALCULATE KMIN. & KMAX.
540 PAGE
550 I=I+1
560 IF X=2 THEN 610
570 REM *** USE EQN. #1
580 GOSUB 1960
590 K=C*Y/B*SQR(W)
600 GO TO 640
610 REM *** USE EQN. #2
620 GOSUB 2080
630 K=C*Y*SQR(A)/B*W
640 K=K/1000
650 K1=K*R
```

TABLE V (Cont'd)

```
[illegible] K2=K-K1
[illegible] PRINT "KMIN. =";K1;" KMAX. =";K
[illegible] L1=0
[illegible] PRINT
[illegible] PRINT "WHICH LOAD RANGE ARE YOU OPERATING IN ?"
[illegible] PRINT
[illegible] PRINT "1000 LBS."
[illegible] PRINT "2000 LBS."
[illegible] PRINT "5000 LBS."
[illegible] PRINT "10,000 LBS."
[illegible] PRINT
[illegible] INPUT K5
[illegible] X1=L1*2047/K5
790 REMARK END POINTS WILL BE ENTERED AS % OF X1
800 PRINT
810 PRINT "PMAX= ";L1;"  VOLTAGE EQUIVALENT= ";X1
820 PRINT
830 PRINT "DO YOU WISH TO BUILD A FLIGHT BLOCK OR USE EXISTING"
840 PRINT "FLIGHT BLOCK?  BUILD=1  CONTINUE=2"
850 INPUT X
860 IF X=2 THEN 990
870 PAGE
880 PRINT "ENTER THE NUMBER OF END POINTS TO BE USED."
890 INPUT W2
900 DIM T(W2)
910 DIM P(W2)
920 PRINT " SELECT THE TIME AT WHICH EACH LOAD OCCURS AND ENTER THE"
930 PRINT "TIME IN SECONDS. REMEMBER T(INITIAL)=0 SO ENTER 0,0."
940 PRINT "SELECT THE LOADS AS % OF PMAX. BUT ENTER AS A DECIMAL VALUE."
950 FOR L=1 TO W2
960 PRINT L;" ";
970 INPUT T(L),P(L)
980 NEXT L
990 PRINT "WHICH WAVESHAPE WILL BE USED ?"
1000 PRINT "1. RAMP - CONSTANT FREQUENCY"
```

TABLE V (Cont'd)

```
1010 PRINT "2. HAVERSINE - CONSTANT FREQUENCY"
1020 INPUT W1
1030 PRINT "ENTER THE DESIRED FREQUENCY."
1040 INPUT F1
1050 PRINT "REMEMBER TO RESET USDATA UNIT."
1060 PRINT "DO YOU WANT TO ACQUIRE DATA? (YES/NO)"
1070 INPUT A$
1080 IF A$<>"YES" THEN 1210
1090 PRINT "START WITH CHANNEL?";
1100 INPUT N1
1110 N1=N1+1
1120 PRINT "NUMBER OF CHANNELS?";
1130 INPUT N2
1140 PRINT "SCAN RATE WITHIN A BLOCK?";
1150 INPUT N3
1160 PRINT "SCAN COUNT WITHIN A BLOCK?";
1170 INPUT N4
1180 PRINT "BLOCK SAMPLING MODE/RATE?";
1190 INPUT N5
1200 GO TO 1260
1210 LET N1=1
1220 LET N2=1
1230 LET N3=217
1240 LET N4=1
1250 LET N5=0
1260 PRINT "Do you want to read a data tape ?   (Y/N)"
1270 INPUT X$
1280 IF X$="Y" THEN 2280
1290 REMARK CALCULATE ACTUAL END POINTS
1300 FOR L=1 TO W2
1310 P(L)=P(L)*X1
1320 NEXT L
1330 N9=1
1340 F2=(T(W2)-T(1))*(F1*2)
1350 D2=INT(F2+0.5)+1
```

TABLE V (Cont'd)

```
1350 DIM H(D2)
1360 S1=W2-1
1370 H(1)=P(1)
1380 FOR L=1 TO S1
1390 F3=(T(L+1)-T(L))*(F1*2)
1400 N=INT(F3+0.5)
1410 L9=(P(L+1)-P(L))/N
1420 FOR K=1 TO N
1430 H(N9+K)=H(N9+K-1)+L9
1440 NEXT K
1450 N9=N9+N
1460 T(L+1)=T(L)+N/(F1*2)
1470 NEXT L
1480 FOR L=1 TO N9
1490 H(L)=INT(H(L)+0.5)
1500 NEXT L
1510 PRINT T
1520 PRINT N9
1530 PRINT H
1540 PRINT "DO YOU WANT TO CREATE A DATA FILE? (Y/N)"
1550 INPUT X$
1560 IF X$="Y" THEN 2380
1570 LET F1=INT(10*F1+0.5)
1580 PRINT "FREQUENCY USED IS:";F1
1600 PRINT @16:2;"/";F1
1610 PRINT @16:3;"/";240
1620 PRINT @16:4;"/";W1
1630 PRINT @16:5;"/";2
1640 PRINT @16:6;"/";N1;"/";N2;"/";N3;"/";N4;"/";N5
1650 DIM B$(5000),B1(100)
1660 B$=""
1670 I=0
1680 M=1
1690 I1=INT(750/(N9-1))*(N9-1)
1700 PRINT "END POINTS PER TRANSFER CYCLE = ";I1
```

TABLE V (Cont'd)

```
1710  I2=1
1720  A$="7"
1730  A$=A$&"/"
1740  E$=STR(H(M))
1750  M=M+1
1760  IF M<N9 THEN 1780
1770  M=1
1780  A$=A$&E$
1790  I2=I2+1
1800  IF I2>I1 THEN 1860
1810  IF LEN(A$)<65 THEN 1730
1820  LET B$=B$&A$
1830  I=I+1
1840  B1(I)=LEN(A$)
1850  GO TO 1720
1860  LET B$=B$&A$
1870  I=I+1
1880  B1(I)=LEN(A$)
1890  PRINT "DATA LINES PER TRANSFER CYCLE = ";I
1900  GOSUB 2190
1910  PRINT @16:8;"/";1;"/";50;"/";60
1920  LET Z2=0
1930  PRINT "ARE YOU READY TO START TEST? IF SO PRESS USER DEFINABLE #1."
1940  LET Z1=0
1950  WAIT
1960  REM *** EQUATION NO. 1
1970  PRINT "THE EQUATION SELECTED IS GOOD FOR H/W=0.6"
1980  PRINT
1990  A=A3+A0
2000  A4=A3
2010  N1=N2
2020  D=A/W
2030  Z6=2+D
2040  Q=0.886+4.64*D↑2+14.72*D↑3-5.6*D↑4
2050  U2=SQR((1-D)↑3)
```

TABLE V (Cont'd)

```
2060 Y=Z6*Q/U2
2070 RETURN
2080 REM *** EQUATION NO. 2
2090 PRINT "THE EQUATION SELECTED IS GOOD FOR H/W=0.486"
2100 PRINT
2110 A=A3+A0
2120 A4=A3
2130 N1=N2
2140 D=A/W
2150 Y=30.96-195.8*D+730.6*D↑2-1186.3*D↑3+754.5*D↑4
2160 RETURN
2170 POLL Q1,Q2;16
2180 IF Q2<>66 THEN 2260
2190 I1=1
2200 FOR I2=1 TO I
2210 A$=SEG(B$,I1,B1(I2))
2220 I1=I1+B1(I2)
2230 PRINT @16:A$
2240 NEXT I2
2250 RETURN
2260 PRINT "THE STATUS WORD IS  ";Q2
2270 GO TO 2570
2280 REM*** THIS ROUTINE GETS DATA FROM THE TAPE                    ***
2290 PRINT "ENTER NUMBER OF FILE THAT CONTAINS THE DATA"
2300 INPUT F7
2310 FIND F7
2320 INPUT @33:N9
2330 DIM H(N9)
2340 FOR L=1 TO N9
2350 INPUT @33:H(L)
2360 NEXT L
2370 GO TO 2670
2380 REM,*** THIS ROUTINE PREPARES DATA FILES
2390 PRINT "ENTER NUMBER OF FILE THAT YOU WISH TO USE"
2400 INPUT F7
```

TABLE V (Cont'd)

```
2410 FIND F7
2420 PRINT @33:N9
2430 FOR I=1 TO N9
2440 PRINT @33:H(I)
2450 NEXT I
2460 GO TO 1580
2470 PRINT "YOU ARE NOW RUNNING FLIGHT BLOCK"
2480 PRINT @16:1;"/";1
2490 PRINT @32,26:2
2500 WAIT
2510 PRINT J9
2520 IF Z2=0 THEN 2540
2530 GOSUB 2710
2540 IF Z1<>0 THEN 1930
2550 J9=J9+1
2560 GO TO 2500
2570 IF Q1=1 THEN 2590
2580 STOP
2590 LET Q2=Q2-64
2600 GOSUB Q2 OF 2630,2650,2650,2670,2670,2670,2670
2610 IF Q2>0 THEN 2600
2620 RETURN
2630 LET Q2=Q2-1
2640 GO TO 2690
2650 LET Q2=Q2-2
2660 GO TO 2280
2670 LET Q2=Q2-4
2680 GO TO 2980
2690 LET Z2=-1
2700 RETURN
2710 PRINT @16:1;"/";6
2720 INPUT @16:Z5
2730 PRINT Z5
2740 LET Z5=Z5/N2
2750 FOR L=1 TO Z5
```

TABLE V (Cont'd)

```
2750 PRINT @16:1;"/";6
2760 INPUT @16:2$
2770 PRINT "A/D  ";Z$
2780 NEXT L
2790 PRINT @16:6;"/";N1;"/";N2;"/";N3;"/";N4;"/";N5
2800 LET Z2=0
2810 RETURN
2820 PRINT "FLIGHT BLOCK STOPPED"
2830 PRINT @16:1;"/";2
2840 RETURN
2850 PRINT "FLIGHT NOW IN HOLDING PATTERN . . . TEST INTERRUPTED"
2860 PRINT @16:1;"/";3
2870 RETURN
2880 PRINT "TEST CONTINUED"
2890 PRINT @16:1;"/";4
2900 RETURN
2910 PRINT @16:1;"/";9
2920 RETURN
2930 PRINT @16:1;"/";5
2940 INPUT @16:K$
2950 PRINT "ELAPSED SEGMENTS   ";K$
2960 RETURN
2970 PRINT "PANIC STOP"
2980 LET Z1=-1
3000 RETURN
3010 PAGE
```

## 2. DETERMINATION OF MECHANICAL PROPERTIES AND RELIABILITY OF STRUCTURAL MATERIALS

A large number of highly diverse and basic experiments were conducted to generate data on the mechanical properties and reliability of structural materials used in airframes and gas-turbine engines in aircraft under a variety of loading and environmental conditions as required in AFML R&D programs. The data were generated on the mechanical behavior with specific emphasis being placed upon the fracture, fatigue, and crack-growth behavior of structural materials for airframes and metal alloys and ceramics for advanced gas-turbine engines. The materials investigated included metal-matrix composites, nickel-base superalloys, ($\alpha$-$\beta$) titanium alloys, high-strength low-alloy steels, structural ceramics, and other structural materials.

The types of mechanical determinations included the following:

1. Room-temperature uniaxial tension and compression tests using Instron testing machines.

2. Creep and uniaxial tension and compression tests at temperatures up to 760°C (1400°F) utilizing Instron and servo-controlled MTS machines and creep frames with both resistance and inductance heating systems.

3. Low-cycle-fatigue crack-initiation experiments at room and elevated temperatures utilizing servo-controlled MTS machines.

4. Sustained-load crack-growth experiments at room and elevated temperatures utilizing Instron, MTS machines, and creep frames or special sustained-load fixtures.

5. Fatigue experiments under cyclic loading utilizing resonant Schenck fatigue machines or servo-controlled MTS machines
   a. to produce a fatigue precrack,
   b. to generate fatigue-crack-growth-rate data (e.g., da/dN vs. K),

c. to determine fatigue life (i.e., S-N curves), and
d. to evaluate the effects upon crack growth of single and multiple overloads and underloads.

6. FCGR experiments under programmable spectrum loading utilizing servo-controlled MTS machines, Wavetek function generators, and U.S. Data Control System.

The reduced and analyzed data generated in this program were used in the following reports and papers:


G. Cloud, "Residual Surface Strain Distributions Near Holes Which Are Coldworked to Various Degrees," AFML-TR-78-153.

J. W. Jones, "The Interferometric Measurement of Near Crack Tip Displacement in a Nickel Base Superalloy at Ambient and Elevated Temperatures," AFML-TR-78-159.

T. Nicholas, J. Barber, and R. S. Bertke, "Impact Damage of Titanium Leading Edges from Small Hard Objects," AFML-TR-78-173.

T. Lynch, "Inhibitor Effectiveness and Inhibition of Environmentally Enhanced Crack Growth Rates in High Strength Steels," AFML-TR-77-202.

A. F. Grandt, Jr. and N. E. Ashbaugh, "Evaluation of a Crack Growth Gage for Monitoring Possible Structural Fatigue Crack Growth," AFML-TR-77-233.

T. K. Moore, "The Influence of Hole Processing and Joint Variables on the Fatigue Life of Shear Joints," AFML-TR-77-167, Vols. I and II.

J. W. Jones, D. E. Macha, and D. M. Corbly, "Observations on Fatigue Crack Opening Load Displacements," Int. J. Frac. 14 (1978).

F. W. Vahldiek, F. Thornton, and C. T. Lynch, "Effects of Temperature and Humidity on Corrosion Fatigue Behavior of 4340 Steel," Presented at AIME 106th Annual Meeting, 1978.

R. C. Donat, "Sustained Load Crack Growth Measurements in IN-100," ASTM E-24.04 Subcommittee on Subcritical Crack Growth, Atlanta, GA, 14 March 1979.

R. C. Donat and L. S. Fu, "Stable Crack Growth in IN-100 at Elevated Temperatures," ASTM Committee E-24 on Fracture Testing Metals, 11th National Symposium on Fracture Mechanics, Virginia Polytechnic Institute, Blacksburg, VA, 13 June 1978.

D. E. Macha, "Fatigue Crack Growth Retardation Behavior of IN-100 at Elevated Temperatures," To be published in Engineering Fracture Mechanics.

D. E. Macha, A. F. Grandt, Jr., and B. J. Wicks, "Effects of Gas Turbine Engine Load Spectrum Variables on Crack Propagation," To be published in ASTM STP resulting from Symposium on Effect of Load Spectrum Variables on Fatigue Crack Initiation and Propagation, San Francisco, CA, 21 May 1979.

D. E. Macha, D. M. Corbly, and J. W. Jones, "On the Variation of Fatigue Crack Opening Load with Measurement Location," To be published in Experimental Mechanics.

T. Nicholas, D. C. Krinke, and J. P. Barber, "The Charpy Impact Test as a Method for Evaluating Impact Resistance of Composite Materials," AFML-TR-78-54.

W. H. Cathey and A. F. Grandt, Jr., "Fracture Mechanics Consideration of Residual Stresses Introduced by Coldworking Fastener Holes," Accepted May 1979 for publication in the Journal of Engineering Materials and Technology.

S. Fujishiro and D. Eylon, "Improved High Temperature Mechanical Properties of Titanium Alloys by Platinum Ion Plating," Thin Solid Films 54, 309 (1978).

S. Fujishiro and D. Eylon, "Titanium and Titanium Alloys Ion Plated with Nobel Metals and their Alloys," U.S. Patent 4,137,370 dated 30 January 1979.

D. Eylon and C. M. Pierce, "Effect of Microstructure on Notch Fatigue Properties of Ti 6Al-4V," Met. Trans. A 7A, 111 (January 1976).

D. Eylon, J. A. Hall, C. M. Pierce, and D. L. Ruckle, "Microstructure and Mechanical Properties Relationship in the Ti-11 Alloy at Room and Elevated Temperatures," Met. Trans. A 7A, 1817 (December 1976).

J. S. Santner and D. Eylon, "Fatigue Behavior and Failure Mechanisms of Modified 7075 Aluminum Alloys," To be published.

I. A. Martorell, "Effects of Isothermal Forging Conditions on the Properties and Microstructures of Ti 10V-2Fe-3Al," AFML-TR-78-114.

J. Awerbuch, "K-Calibration of Unidirectional Metal Matrix Composites," J. Composite Mat. 12, 222 (1978).

J. Awerbuch and H. T. Hahn, "Hard Object Impact Damage of Metal Matrix Composites," J. Composite Mat. 10, 231 (1976).

J. Awerbuch and H. T. Hahn, "Fatigue and Proof Testing of Unidirectional Graphite/Epoxy Composite," To be published.

C. T. Lynch, F. W. Vahldiek, K. J. Bhansali, and R. Summitt, "Inhibition of Environmentally Enhanced Crack Growth Rates in High Strength Steels," Presented at the Symposium on Environment Sensitive Fracture of Engineering Materials, AIME Meeting, Chicago, IL, 26 October 1977.

J. A. Ori and A. F. Grandt, Jr., "Single-Edge-Cracked Crack-Growth Gage," Paper accepted for publication in ASTM STP 677 Fracture Mechanics, Proceedings of 11th National Symposium on Fracture Mechanics, sponsored by ASTM Committee E-24, Virginia Polytechnic Institute and State University at Blacksburg, Blacksburg, VA June 1978, In press.

K. S. Mazdiyasni and R. Ruh, "High/Low Modulus Composite for Improved Mechanical Properties," Presented at the 80th Annual Meeting and Exposition of The American Ceramic Society, Detroit, MI, May 1978.

J. Awerbuch and H. T. Hahn, "Crack-Tip Damage and Fracture Toughness of Boron/Aluminum Composites," J. Composite Mat. 13 (April 1979).

J. Awerbuch and H. T. Hahn, "Crack-Tip Damage and Fracture Toughness of Borsic/Titanium Composite," To be published.

J. Awerbuch, "Failure Mechanism and Deformation Characteristics of Unidirectional Boron Aluminum Composites," To be published.

J. Awerbuch, "Notched Sensitivity of Boron Aluminum Laminate," To be published.

J. Awerbuch, "Fracture Behavior of Boron Aluminum and Borsic Titanium Composites," To be published.

## 3. IMPROVEMENTS TO THE FACILITY

The following discussion concerns certain pieces of equipment and instrumentation which were fabricated and assembled to improve and expand the capabilities and flexibility of the Mechanical Test Facility.

### a. Hydraulic-Pump Installation

Extensive changes were made to the hydraulic system which is used to actuate the test frames in the laboratory. In the normal mode of

operation, the new system is powered by a single variable flow pump with 70-gpm capacity. In order to provide convenient dispersal and collection of hydraulic fluid and to facilitate the incorporation of future frames in the laboratory, manifolds were placed in the hydraulic supply system. The operation of each of the seven frames requires a high-pressure (3000-psi) inlet line, a low-pressure (≈ 800-psi) return line, and a drain line. These lines from several frames were brought together at a manifold which is composed of three blocks--a high-pressure block, a low-pressure block, and a return block. From each of these blocks of the manifolds (currently there are two), lines are plumbed to a central manifold at the pump. Figure 1 is a schematic of the pump, lines, manifolds, and frames for normal mode of operation. For clarity, the drain lines which parallel the other hydraulic lines are not shown in the figure. The seven frames are denoted by a number in conjunction with the symbol KIP and the pump by 70 GPM.

In the previous hydraulic system, each frame was actuated by its own pump except for two frames which were actuated by a 20-gpm pump. In the new system these pumps can be connected for a standby mode of operation when the 70-gpm pump is inoperable.

In the design and construction of the new system, the following improvements and considerations were made:

1. A single pump for all test frames was incorporated to reduce pump cost on future test-system purchases and to avoid maintenance requirements on a number of pumps. The pump is of sufficient capacity to supply the flow rates required for additional frames.

2. Manifolds were designed and incorporated into the system for distributing adequate flow to the individual frames.

3. Dual high-pressure lines [1.91-cm- (3/4-in.-) o.d. stainless steel] and dual return lines [2.54-cm- (1-in.-) o.d. stainless steel] were installed from the central manifold to

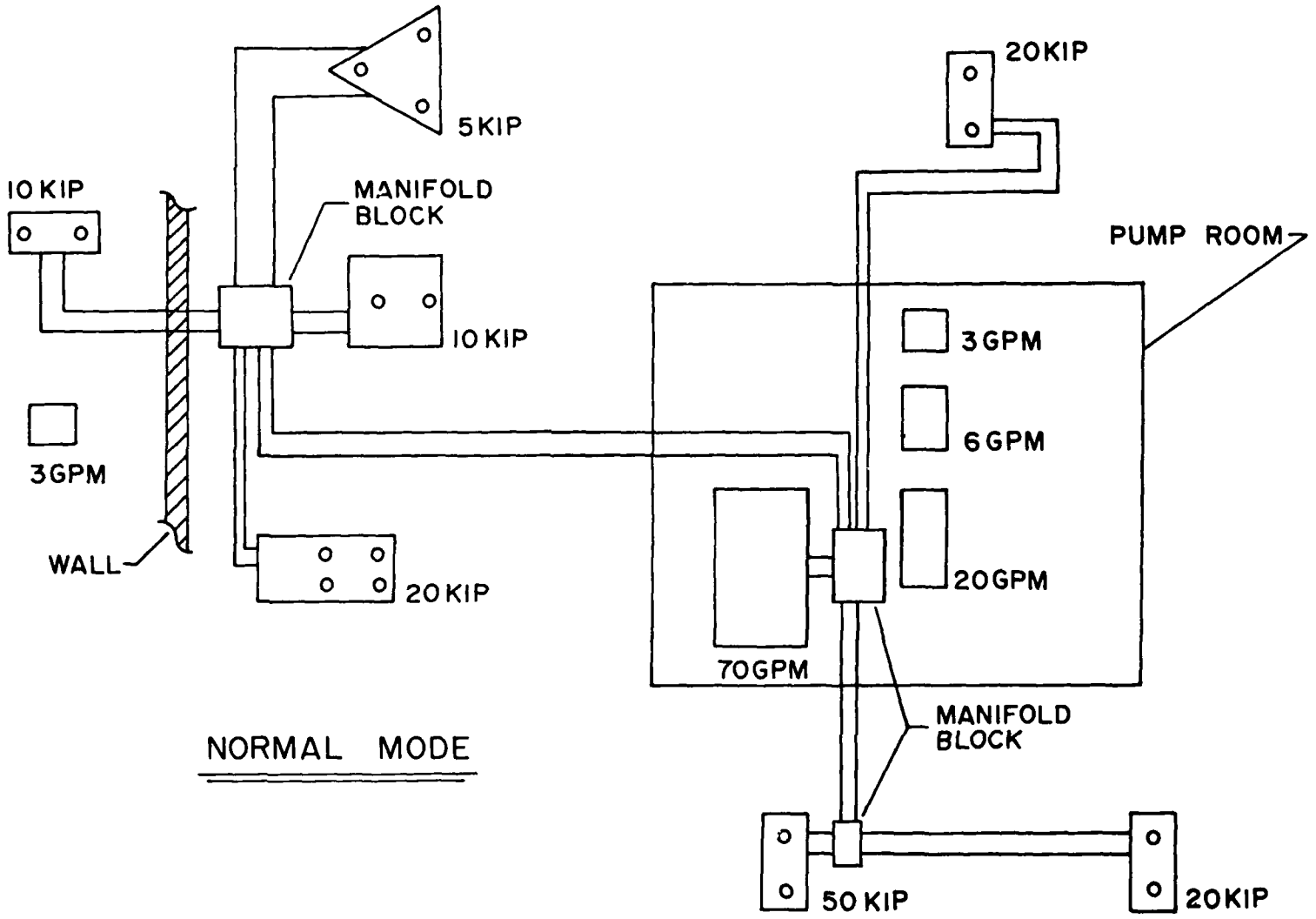


Figure 1. New Pump Configuration for Normal-Mode Operation

the two outlying manifolds in order to accommodate the high flow rates which would be required for certain tests. An adequate supply of hydraulic fluid is necessary to reduce the interaction (i.e., cross-talk) among test frames. Also, the cost of the dual lines was less than that of a single line which would carry an equivalent flow rate, and the installation of each of the dual lines by flaring and fitting was less costly than a single line which would have required welding.

4. To reduce vibration and noise in the system, flexible hoses were used to connect the pump to the central manifold and the hydraulic lines to the linetamers on the individual frames. In the previous system the frames had been hard plumbed to the lines. The linetamer on each frame provides control of the pressure requirements for the individual frame.

   In order to minimize pump noise, the wall and ceiling joints of the pump room have been caulked and the floor trenches under the pump room walls filled with expandable foam.

5. In order to keep the cost of the system as low as possible, extra pumps for the standby mode of operation must be manually connected to the hydraulic lines and central manifold rather than use expensive high-pressure valves to switch from normal mode to standby mode.

Currently, normal mode is being used now that adequate power (168 amps maximum at 440 V) has been brought into the laboratory to operate the 70-gpm pump.

b. Three- and Six-Channel d.c. Conditioners

During development on an earlier contract of the pulse-width-delay circuit for the slit Hopkinson pressure-bar system, a need for a stress or strain signal-conditioning circuit was recognized. For flexibility the signal-conditioning circuit allows the gain factor to be set on each channel and provides a switch to select a four-, two-, or one-active-arm bridge condition. A zero switch is also provided to reference true zero. For calibration a precision resistor is switched across one arm of the bridge to provide a simulated strain output. Full-scale calibration can be made without a zero shift. The circuitry of the conditioner has an extremely low noise-to-signal ratio and provides a stable output signal. Excitation is fixed at 7.0 V d.c. The conditioner has been packaged into either a basic three-channel conditioner with a pulse-width-delay integrator circuit and three channels of d.c. signal conditioning or six channels of d.c. signal conditioning without the integrator circuit.

The versatile conditioner has been used with many different types of transducers. The most common applications are for resistive extensometers, resistive strain gages bonded directly to specimens, axial load transducers, resistive torque cells, displacement gages, direct-current differential transducers (DCDT), and stroke transducers. Three six-channel and one three-channel conditioners have been assembled. Most components for building an additional six-channel conditioner are available.

c. Development of an SRL d.c. Conditioner for the MTS Control Console

A d.c. conditioner was specifically designed to be a direct replacement for the MTS conditioner Model 440-21 or 440-22. The MTS-supplied conditioner was found to be limited in use and difficult to set up. Changes in the MTS-conditioner excitation voltage interacted with the scale calibration which resulted in a great deal of time being spent on calibration.

The SRL d.c. conditioner was designed to eliminate the above problems and improve the flexibility of this type of d.c. conditioner. The

convenient feature of the conditioner is that it permits selection of a four-, two-, or one-active-arm bridge condition with a switch. A zero switch is also provided to reference true zero. A calibration resistor is provided which, when activated, is inserted across one arm of the bridge circuit to provide a simulated strain output. Full-scale calibration can be made without a zero shift. Excitation is fixed at 7.0 V d.c. This conditioner can be used with the same types of transducers as the three- and six-channel d.c. conditioners. Four of these conditioners have been assembled.

d. Furnaces for Elevated-Temperature Testing and Power Controllers

Design and fabrication of four furnaces for use in the elevated-temperature (up to 1500°C) tests at the AFML Mechanical Test Facility have been completed, and components for a fifth furnace have been fabricated. The furnaces were designed primarily for elevated-temperature testing of compact-tension specimens. The size of the heated zone of a furnace is dictated by the type of specimen to be tested and can be altered by increasing or decreasing the outer-shell dimensions while retaining the temperature capability.

Windows were designed into the furnace permitting use of a variety of optical-observation equipment such as film-recording cameras and video cameras with tape and visual systems. One furnace, which was specifically designed for laser-interferometric gage work, has three windows in each half of the furnace. The center window permits laser light entry to the furnace, and the upper and lower windows permit exit of the reflected interference beams. Type K-thermocouples were used to monitor and control the temperature in the heated zone. The thermocouples can be placed on the specimen or anywhere in the heated zone as requirements dictate.

The furnace supports can be mounted on the MTS test frames and on the creep frames in the laboratory. Ports other than windows can be put into special locations, enabling clip gages and extensometers to be used for measurements.

General specifications and operating characteristics of these furnaces are listed below:

Power:

220 V a.c., 30 amp

Type of Elements:

Refractory-contained helically wound coils of Kanthal alloy

Operating Range:

0 - 1500°C continuous

Temperature Uniformity in Specimen:

± 1°C throughout operating range

Two power controllers were designed and built from the following components:

Barber-Colman zero crossover-firing, time-proportioning power controllers

Barber-Colman digital-set-point controller for driving the power control.

## SECTION III

## APPLICATION OF SOLID MECHANICS TO FAILURE PREDICTION

### 1. CREEP-FATIGUE INTERACTION

Due to anticipated higher operating temperatures, components in gas-turbine engines will experience more severe operating conditions. Therefore, in addition to the fatigue process of the material which must be taken into account, the design of the engine must consider the effects of creep (time-dependent deformation) and the interaction of the creep phenomena and the fatigue process. As a result of the higher temperatures, the useful life of critical components is significantly degraded to $10^4$ - $10^5$ cycles. Since this number of cycles is within the upper range of application of low-cycle fatigue (LCF) models, an examination and subsequent assessment of these models in the prediction of the lifetime was conducted. Several studies which were undertaken to evaluate the modeling of creep-fatigue interactions in Ni-base superalloys are described below.

#### a. Application of Strainrange Partitioning to René 95

A research program was conducted to examine the applicability of the Strainrange Partitioning (SRP) Method for predicting high-temperature, low-cycle-fatigue (LCF) crack initiating. Strain-controlled LCF tests were performed at 649°C (1200°F) on René 95, a high-strength Ni-base superalloy; and SRP was used to correlate the data as well as to predict the number of LCF cycles to failure for a series of validation tests. The data indicate that for René 95, compressive dwell cycles are more damaging than tensile dwell cycles and that the LCF behavior depends largely upon the time in tension per cycle and upon the value of the maximum tensile stress. SRP was unable to satisfactorily predict the cyclic life for several types of LCF tests because the model is not capable of accounting for certain aspects of the cyclic behavior of the alloy, particularly the development of mean stresses.

The results of this program were reported in Air Force Materials Laboratory Technical Report AFML-TR-78-118 entitled, "An Analysis of the

Low-Cycle-Fatigue Behavior of the Superalloy René 95 by Strainrange Partitioning," dated November 1978, and also in an article of the same title in Advisory Group for Aerospace Research and Development Report AGARD-CP-243, entitled, "Characterization of Low-Cycle High-Temperature Fatigue by the Strainrange Partitioning Method," dated April 1978.

b. An Evaluation of Four Creep-Fatigue-Interaction Models

In this program four current models for the creep-fatigue interaction were evaluated for their ability to predict fatigue behavior at 650°C (1200°F) of the thermomechanically processed René 95--an advanced Ni-base superalloy used for turbine disks. These models are the Strainrange-Partitioning Model, the Frequency-Separation Model, the Ostergren Model, and the Damage-Rate Model. A series of strain-controlled fatigue tests was conducted to evaluate these models--continuously cycling tests at two different frequencies, various types of strain-hold tests, and dual-rate continuously cycling tests. These fatigue tests were divided into two groups--baseline tests and verification tests. The baseline tests were used to determine the constants in the models and the correlation ability of the models. The verification tests were used to determine the predictive ability of the models. The best correlation of the baseline tests was to within a scatter band of ± 3.6 and was achieved by the Frequency-Separation Model and the Ostergren Model. The other two models had scatter bands greater than ± 5. The best prediction of the verification tests was to within a factor of ± 5.2 and was achieved by the Ostergren Model. The other models predicted the verification tests from factors of ± 6.1 to ± 18. Each of the models consistently overpredicted or underpredicted the lives of certain types of tests that form the data base. Based upon the results of this study, it was concluded that these models in their present form could not adequately predict the fatigue life of René 95 at 650°C (1200°F).

More detailed information can be found in Air Force Materials Laboratory Technical Report AFML-TR-79-4075 entitled, "An Evaluation of Four Current Models to Predict the Creep-Fatigue Interaction in René 95."

c. Low-Cycle-Fatigue-Model Development

A Stress-Strain-Time Model (SST) was developed to predict high temperature, low-cycle fatigue life. The model incorporates three variables--stress, strain, and time--which were combined in a power-law equation to predict the life. The stress parameter accounts for mean stress effects. The strain parameter accounts for time-independent fatigue damage, and the time parameter accounts for the time dependence upon fatigue life. High-temperature, low-cycle fatigue data for several alloy systems are correlated to within a factor of 2.1, and data predicted to within a factor of 2.6 using t SST Model. The results of this effort will be published in Air Force Materials Laboratory Technical Report AFML-TR-79-4114, entitled, "A Stress-Strain-Time Model (SST) for High-Temperature, Low-Cycle Fatigue," and will be published in the Journal of Engineering Materials and Technology.

d. Crack Initiation Occurring at 5% or 10% Decrease in Load Range

In the evaluation of state-of-the-art models for the creep-fatigue interaction, the experimentally determined lifetimes, $N_f$, were based upon the number of cycles to failure of the specimen, i.e., separation of the specimen into two or more pieces. At least two processes occur during a test--the initiation of a macrocrack in the specimen and the growth of the crack to a critical size when the specimen fails. A question arises as to the appropriateness of a model in characterizing different processes during the fatigue test.

In order to investigate the influence of the initiation and crack-growth processes upon the models, the portions of the lifetime of the specimen spent in these processes must be determined. First, it was assumed that the lifetime to failure of a specimen was composed only of the time required to initiate a macrocrack and the time required to grow the crack to a critical size. The time or cycles required to initiate a crack under strainrange control was determined by the following three similar criteria:

1. When the maximum tensile load began to deviate from a pattern established during the test.

2. When the maximum tensile load deviated by 5% from an established pattern.

3. When the maximum tensile load deviated by 10% from an established pattern.

These three criteria yielded successively higher values of initiation lives, i.e., if the cyclic lifetimes for the above criteria were denoted as $N_i$, $N_5$, and $N_{10}$, respectively, then

$$N_i < N_5 < N_{10} < N_f.$$

For most of the tests which were conducted by Mar-Test of Cincinnati, Ohio, values of $N_i$ have been reported. These values have been compared to the strip-chart traces of load to determine whether they correspond to the initial deviation of maximum tensile load from an established pattern. The results for $N_i$ are presented in Table VI. Generally, the loading pattern which was established during the tests indicated that René 95 softened throughout the entire test. For the above criteria, the tensile load normally decreased more rapidly due to a macrocrack having formed than as a result of strain softening.

However, as can be seen from the comments in Table VI, the initiation lifetimes did not necessarily correspond to a more rapid rate of decrease in tensile load. The anomalies in the tensile-load behavior, inelastic strain, etc., which are noted in the comments have been attributed to the formation of a crack in the vicinity of the contact points of the diametral extensometer. The deformation around the crack was significantly altered, which caused the extensometer to behave erratically. Although the expected decrease in tensile load did not occur, the measured lifetime at the anomalies was still associated with formation of a macrocrack.

TABLE VI

INITIATION LIFETIMES FOR LOW-CYCLE-FATIGUE SPECIMENS

| Specimen | Type Test | $N_i$ (cycles) | $N_f$ (cycles) | $N_i/N_f$ | Comment No.[a] |
|---|---|---|---|---|---|
| 21 | 20 cpm | 198 | 203 | 0.98 | Chart missing |
| 17 | 20 cpm | 227 | 234 | 0.97 | 1 |
| 18 | 20 cpm | 283 | 307 | 0.92 | 3 |
| 22 | 20 cpm | 432 | 461 | 0.94 | 1 |
| 26 | 20 cpm | 700 | 784 | 0.89 | 1 |
| 27 | 20 cpm | 1,406 | 1,629 | 0.86 | 1 |
| 29 | 20 cpm | 4,428 | 5,158 | 0.86 | 1 |
| 30 | 20 cpm | 15,174 | 16,215 | 0.94 | 1 |
| 224 | 20 cpm | 375 | 415 | 0.90 | 1 |
| 221 | 20 cpm | 8,096 | 8,406 | 0.96 | 2 |
| 234 | 20 cpm | 16,560 | 19,160 | 0.86 | 2 |
| 235 | 20 cpm | 21,364 | 22,364 | 0.96 | 2 |
| 5 | 1-0 | 235 | 255 | 0.92 | 1 |
| 10 | 1-0 | 225 | 257 | 0.88 | 1 |
| 7 | 1-0 | 733 | 748 | 0.98 | 4 |
| 12 | 1-0 | 1,246 | 1,289 | 0.97 | 1 |
| 39 | 1-0 | 1,558[b] | 1,781 | 0.87 | 1 |
| 38 | 1-0 | 4,565[b] | 5,013 | 0.91 | 1 |
| 33 | 1-0 | 9,221 | 9,609 | 0.96 | 2 |
| 23 | 0.05 cpm | 105 | 110 | 0.95 | 2 |
| 24 | 0.05 cpm | 138 | 159 | 0.87 | 1 |
| 20 | 0.05 cpm | 295 | 301 | 0.98 | 5 |
| 25 | 0.05 cpm | 277 | 282 | 0.98 | 1 |
| 34 | 0.05 cpm | 495[b] | 526 | 0.94 | 1 |
| 19 | 0.05 cpm | 1,120[b] | 1,138 | 0.98 | 2 |
| 6 | 0-1 | 198 | 207 | 0.96 | 2 |
| 11 | 0-1 | 124 | 209 | 0.59 | 3 |
| 14 | 0-1 | 168 | 219 | 0.77 | 1 |
| 8 | 0-1 | 353 | 413 | 0.85 | 3 |
| 13 | 0-1 | 725 | 846 | 0.86 | 1 |
| 16 | 0-1 | 3,028 | 3,093 | 0.98 | 2 |
| 233 | 0-1 | 6,233 | 6,519 | 0.96 | 1 |
| 40 | 10-0 | 1,550[b] | 1,705 | 0.91 | 1 |
| 228 | 10-0 | 441 | 481 | 0.92 | 1 |
| 28 | 10-10 | 113[b] | 115 | 0.98 | 2 |
| 31 | 10-10 | 190 | 199 | 0.95 | 1 |
| 230 | 10-10 | 317 | 331 | 0.96 | 1 |

TABLE VI (Cont'd)

| Specimen | Type Test | $N_i$ (cycles) | $N_f$ (cycles) | $N_i/N_f$ | Comment No.[a] |
|---|---|---|---|---|---|
| 41 | 0-10 | 244[b] | 283 | 0.86 | 1 |
| 222 | 0-10 | 204 | 224 | 0.91 | 1 |
| 223 | 10-1 | 923 | 945 | 0.98 | 1 |
| 227 | 10-1 | 416 | 455 | 0.91 | 1 |
| 225 | 1-10 | 434 | 464 | 0.94 | 1 |
| 226 | 1-10 | 344 | 349 | 0.99 | 1 |
| 1 | 1-1 | 156 | 156 | 1.00 | 4 |
| 2 | 1-1 | 236[b] | 238 | 0.99 | 2 |
| 32 | 1-1 | 303 | 358 | 0.85 | 1 |
| 9 | 1-1 | 839 | 959 | 0.87 | 1 |
| 4 | 1-1 | 1,118 | 1,215 | 0.92 | 1 |
| 15 | 1-1 | 1,175 | 1,288 | 0.91 | 3 |

(a) Comments on the measured point of initiation:

1. $N_i$ occurs at the point where the rate of softening increases, as evidenced by the decrease in $F_t$.
2. $N_i$ occurs at the point where $F_t$ begins to increase more rapidly.
3. No apparent change at $N_i$.
4. $N_i$ occurs at the point where the plastic strain, $\varepsilon_p$, begins to increase more rapidly.
5. No statement due to irregularity in chart (variation ± 500 lb cycle to cycle last 5% of test history).

(b) No value reported by Mar-Test.

As can be noted in Table VI, the ratio of initiation life to failure life was generally above 90%. Thus, it was concluded that the initiation process represents the predominant portion of the life of the specimen. As a result of this high ratio, the use of initiation lives rather than failure lives in the evaluation of the models had a negligible effect upon the scatter band for predicted lives as a function of observed life. In addition, the use of initiation lives rather than failure lives did not eliminate the larger scatter which had occurred with certain specimens, e.g., 33 and 18.

In conclusion, the use of initiation lives rather than failure lives in state-of-the-art models when applied to René 95 did not provide a more consistent basis upon which to evaluate the predictability of the models.

## 2. EVALUATION OF A CRACK-GROWTH GAGE

An experimental and analytical investigation was conducted on the use of a precracked coupon mounted onto a structure for monitoring the effect of service loads upon fatigue-crack growth in the structure. The precracked coupon or "gage" is a simple device which provides a convenient means for determining the potential damage in a structure since the gage takes into account the mechanics of crack growth. Experimental results were reported for gages made from two aluminum alloys and having two types of crack geometries. These gages contained either a center crack or a single crack at the edge of a hole. The effect of the load amplitude upon the growth of the crack in the gage as a function of the crack growth in the structure was investigated. All tests were conducted under constant-amplitude cyclic load. A theoretical model was developed to predict the correlation between the growth of the cracks in the gage and in the structure. Two areas of major importance in the analysis were the load transfer from the structure through the ends of the crack gage and the crack-propagation law for the crack growth in the gage and in the structure. Comparison of the analyses and the experimental results was made. Details of the work were reported in Air Force Materials Laboratory Technical Report AFML-TR-77-233 entitled, "Evaluation of a Crack-Growth Gage for Monitoring Possible Structural Fatigue-Crack Growth," and in American Society for Testing and Materials STP671 entitled, Service Fatigue Loads Monitoring, Simulation, and Analysis, dated 1979.

## 3. ANALYSIS OF STRIP CONTAINING AN ECCENTRIC CRACK

Analysis and determination of expressions for computer calculations for the stress-intensity factors at the tips of an eccentric crack in a strip was performed. Two sets of expressions were obtained--one applies to the problem of an infinitely long strip under uniform tension and the other to the problem of a finite-length strip under uniform displacement. The geometrical parameters used for the problem are indicated on the schematic of the strip in Fig. 2 and are described below.

For the eccentric-crack problem, two parameters are required for describing the location of the crack rather than one parameter as in the case of the center crack where the eccentricity, E, is zero. It was convenient for the development of the expressions to use a nondimensional eccentricity

$$e' \equiv 2E/W \tag{1}$$

and a nondimensional pseudo-crack length

$$g' \equiv a/(W/2 - E), \tag{2}$$

where a is the half crack length, W is the width of the strip, and E is the distance between the centerline of the strip and the middle of the crack. The distance E was assumed to be positive when the middle of the crack was to the right of the centerline of the strip. However, no loss of generality occurred when E was restricted to non-negative values since a negative E from the front of the strip corresponded to a positive E when viewed from the back side of the strip. Thus, for the analysis the ranges of the nondimensional parameters were $0 \leq e' < 1$ and $0 \leq g' < 1$. For any nonzero value of e' then, as $g' \to 1$, the right crack tip approached the right edge of the strip but the left crack tip remained a finite distance from the left edge of the strip. A center-cracked strip corresponds to $e' = 0$.

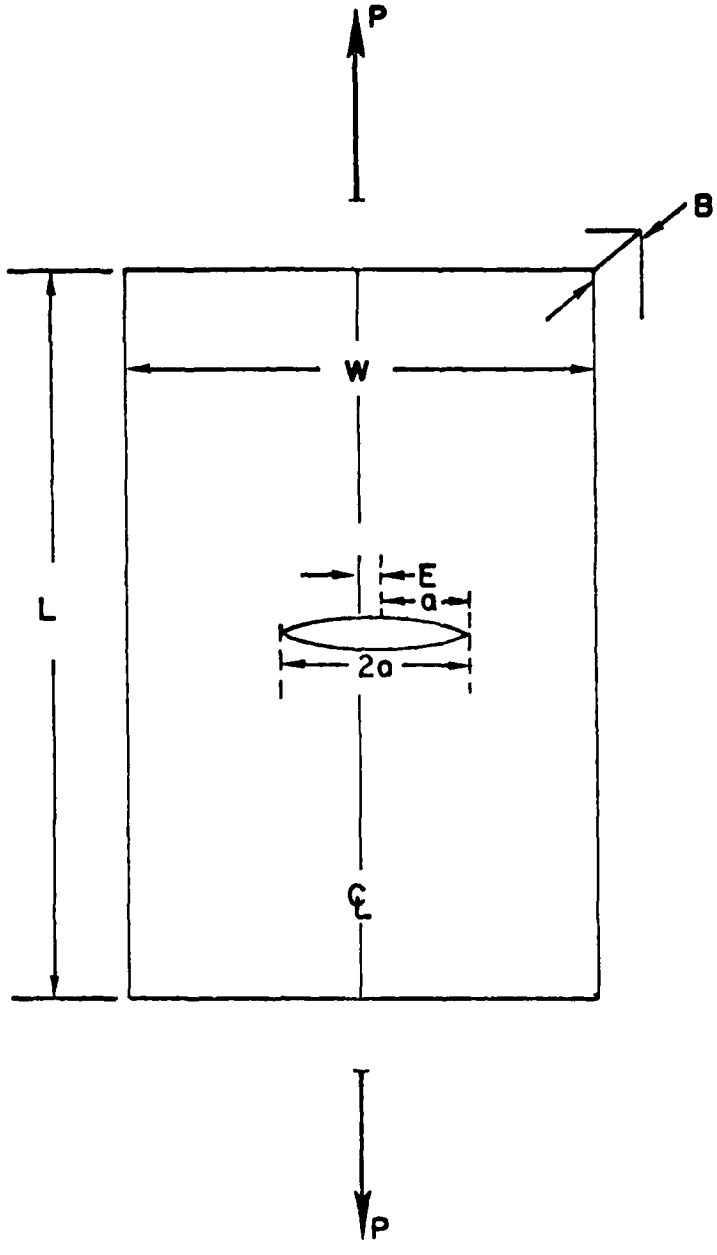


Figure 2. Schematic of an Eccentrically Cracked Strip

For an infinitely long strip ($L \to \infty$, see Fig. 2), the analytical solution to the problem had been obtained in the form of a singular integral equation.[5] The values of the stress-intensity factors were determined from a numerical evaluation of the integral equation[1] (report for the period 15 October 1978 through 15 January 1979).

The form of the functional expressions which were used to fit the computed values of the stress-intensity factors, K, for the infinitely long strip under uniform stress, $\sigma_o \equiv P/(BW)$, was

$$K^+/(\sigma_o\sqrt{\pi a}) = [1 + a_2^+(e')g'^2 + a_4^+(e')g'^4]/\sqrt{\cos(\tfrac{\pi}{2}\, g')}\ , \qquad (3a)$$

and

$$K^-/(\sigma_o\sqrt{\pi a}) = [1. + a_0^-(e')e' + a_2^-(e')g'^2 + a_4^-(e')g'^4]/[\sqrt{\cos(\tfrac{\pi}{2}\, g')} + a_0^-(e')e'], \qquad (3b)$$

where $a_2^+$, $a_4^+$, $a_0^-$, $a_2^-$, and $a_4^-$ are functions of the nondimensional eccentricity. These functional forms were chosen in order that both the proper singular behavior of $K^+$ and the bounded behavior of $K^-$ would be obtained as $g' \to 1$. When determining the functions a(e'), it is noted that Eqs. (3a) and (3b) must be equivalent for $0 \leq g' < 1$ when $e' = 0$, which corresponds to the center-cracked strip.

In an attempt to provide K-expressions which would be applicable for large ranges of e' and g' values, the functional forms of the a's in (3) became extremely complicated. In order to determine the best fit for these coefficients as a function of e', it was necessary to employ nonlinear expressions for the $a^-$ coefficients. The expressions for the a-functions which were obtained from a least-square fit to the analytical results became

$$a_2^+(e') = -0.023609 - 0.86494319\ e' + 3.92897942\ e'^2 - 6.28039\ e'^3 + 2.96346056\ e'^4 ,$$

$$a_4^+(e') = 0.059662 + 1.0787413\ e' - 4.1324643\ e'^2 + 4.05368446\ e'^3 - 1.1984057\ e'^4 , \tag{4a}$$

and

$$a_0^-(e') = 1.3136 + 23.117\ e^{-11e'} \sin[\frac{2\pi}{0.75}(e' + 0.03)],$$

$$a_2^-(e') = 0.017563 + 0.36773\ e^{-5e'} \sin[\frac{2\pi}{0.56}(e' - 0.01)], \tag{4b}$$

$$a_4^-(e') = -0.22063 + 0.73243\ e^{-10e'} \sin[\frac{2\pi}{0.56}(e' + 0.035)].$$

After substitution of (4a) and (4b) into (3a) and (3b), respectively, the computed functional values of the stress-intensity factors were compared to the analytical values. This comparison showed that the functional expressions (3a) and (3b) provided a computational accuracy producing less than 1% error for $0 \leq e' \leq 0.8$ and $0 \leq g' \leq 0.8$ and less than 3% error for $0 \leq e' \leq 0.8$ and $0 \leq g' \leq 0.909$.

For the finite-length strip (L/W = 4 in Fig. 2) where the ends are clamped and a uniform displacement perpendicular to the crack was applied, the stress-intensity factors at the crack tips for various values of e' and g' were determined through the application of boundary integral equations. Details of the development of the solution from the boundary integral equation (partially funded under this program) were presented in a paper entitled, "An Integral-Equation Solution for a Bounded Elastic Body Containing a Crack: Mode I Deformation," which was published in the International Journal of Fracture (Vol. 14, dated 1978). The analytical values were given in Ref. 1 (report for the period 15 October 1978 through 15 January 1979). For the evaluation of $\sigma_o$ in (3) for this problem, the normal stress distribution at the end obtained from the numerical solution was integrated in order to determine the load P. For g' = 0, the analytical results were assumed to be sufficiently close the unity, which

also appeared to be a reasonable value for the extrapolation of the analytical data for $g' > 0$.

The analytical values indicated that the stress-intensity factor at the tip nearer the edge ($K^+$) increased more rapidly than $K^-$ as the eccentricity increased. This result was similar to that obtained for the eccentric crack in an infinitely long strip under uniform-stress boundary conditions at the ends. However, the rate of increase of $K^+$ as e' increased for a given g' value was higher for the problem with uniform-stress boundary conditions than for the problem with uniform-displacement boundary conditions. An implication of this result was that an eccentric crack would become more eccentric, (i.e., e' would continue to increase) as it grew longer.

The functional expressions which were used to fit the analytical results for the eccentric crack in the finite-length strip were the same [(3a),(3b)] as those used for the infinitely long strip. However, the range of the parameter e' was reduced in order to permit the use of polynomial expressions for the $a^-$ functions in (3b). The range $0 \leq e' \leq 0.1$ appeared to be adequate for resolving some preliminary experimental data. The following expressions were obtained from a least-square fit of the analytical results:

$$a_2^+(e') = -0.047708 - 0.86709\, e' + 2.1064\, e'^2 - 3.6269\, e'^3,$$

$$a_4^+(e') = 0.032552 + 0.16679\, e' - 0.9061\, e'^2 + 3.4054\, e'^3, \qquad (5a)$$

and

$$a_0^-(e') = 0.\ ,$$

$$a_2^-(e') = -0.047708 - 0.85754\ e' - 4.6491\ e'^2 + 34.744\ e'^3, \tag{5b}$$

$$a_4^-(e') = 0.032552 - 6.2647\ e' + 59.818\ e'^2 - 245.15\ e'^3,$$

After substitution of (5a) and (5b) into (3a) and (3b), respectively, the computed values of the nondimensional stress-intensity factors were compared to the analytical values. This comparison showed that the functional expressions (3a) and (3b) along with (5a) and (5b) provide a computational accuracy producing less than 1% error for $0 \leq e' \leq 0.1$ and $0 \leq g' \leq 0.8$. Also values of the stress-intensity factors were computed for $e' = 0.15$ and compared to the corresponding analytical values which were not used in the least-square fit determinations of the coefficients in (5a) and (5b). The computational accuracy for the extrapolation created at most a 2% error.

The expressions (3a) and (3b) for $K^+$ and $K^-$ with substitution of either (4a) and (4b) or (5a) and (5b) have been incorporated into a computer program which can be applied to experimental data on fatigue-crack growth to obtain cyclic crack-growth rates and stress-intensity factors. This computer program was used to reduce data obtained from an experimental study of the retardation effects on crack growth due to overloads and underloads.[6]

## 4. FINITE-ELEMENT ANALYSIS

The major effort in the area of finite-element analysis was directed toward providing operational codes which would be employed in the development of crack-growth modeling and testing.

a. Two-Dimensional Linear-Elastic Analysis

Two-dimensional finite-element codes (see pp. 17 and 26 in Ref. 1 for period 15 October 1978 through 15 January 1979) were developed and evaluated to provide an efficient and accurate linear-analysis scheme which would have the following applications:

1. To provide support in the design and development of experimental tests.

2. To provide COD, load-line displacement, and $K_I$ values for specimen geometries (such as compact and modified compact specimens).

3. To aid in the design of nonstandard specimens (such as ring specimens).

For the purpose of specimen analysis, eight-noded quadrilateral-element formulation using Reissner's Variational Principle (Program No. 4, p. 17, in Ref. 1 for period 15 October 1978 through 15 January 1979) was found to be most suitable. For a typical specimen geometry such as a compact specimen, the average cost per analysis is roughly $0.60. A similar analysis using the NASTRAN can range between $15 and $20.

The accuracy of the program was evaluated by analyzing some specimen geometries for which widely accepted results are available in the literature. These other analytical results and the experimental results are discussed in more detail in the following subsection on compliance concepts. Figure 3 is a comparison of results for a three-point bend specimen. In Fig. 3 the compliance C is associated with the displacement of the load P shown in the insert in the figure. The experimental results are tabulated in Table III of the next subsection. In Fig. 4 results for a compact-tension test specimen are shown.

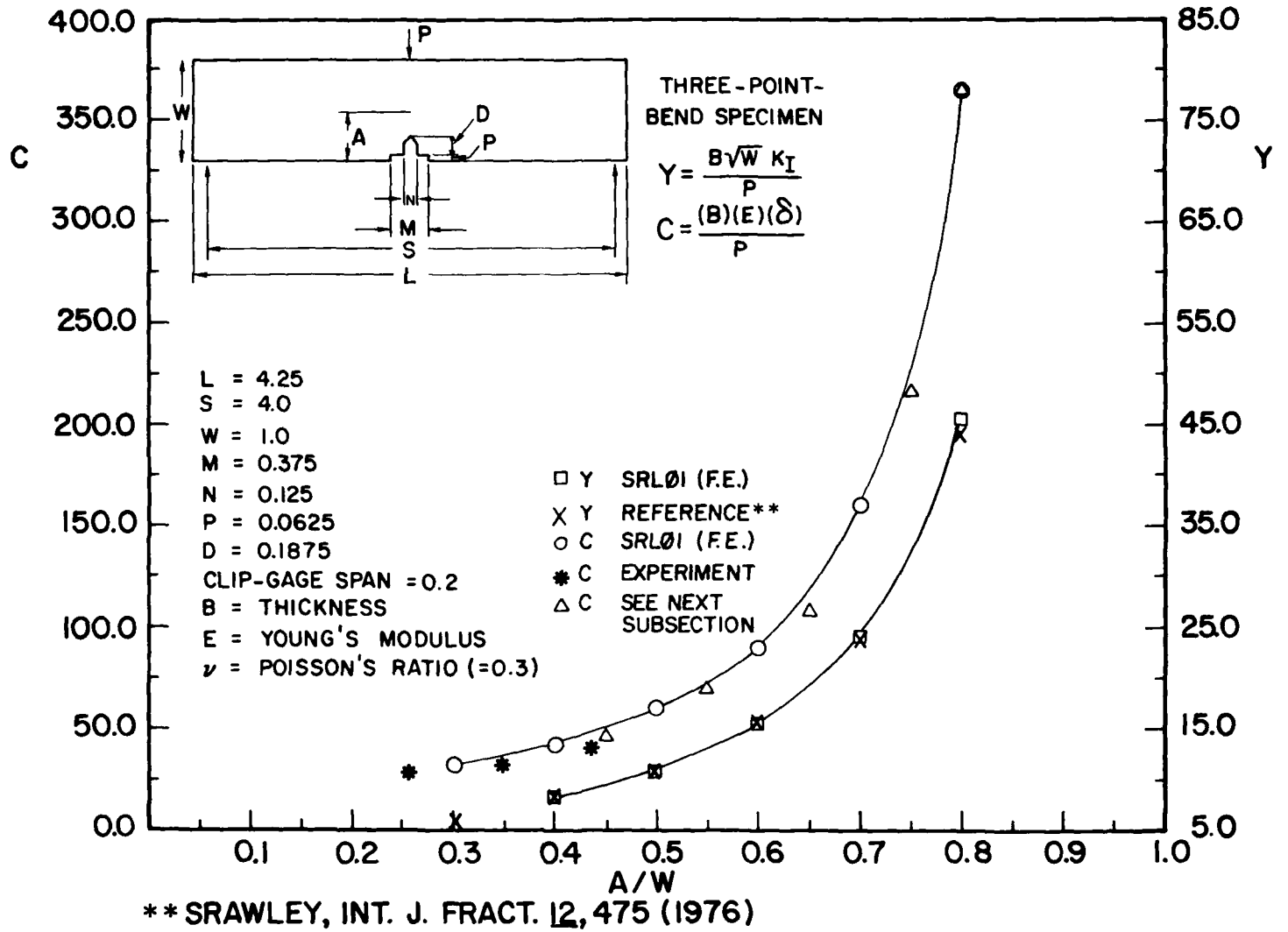


Figure 3. Analytical and Experimental Values of Nondimensional Compliance and Stress-Intensity Factor for Three-Point-Bend Specimen, S/W = 4

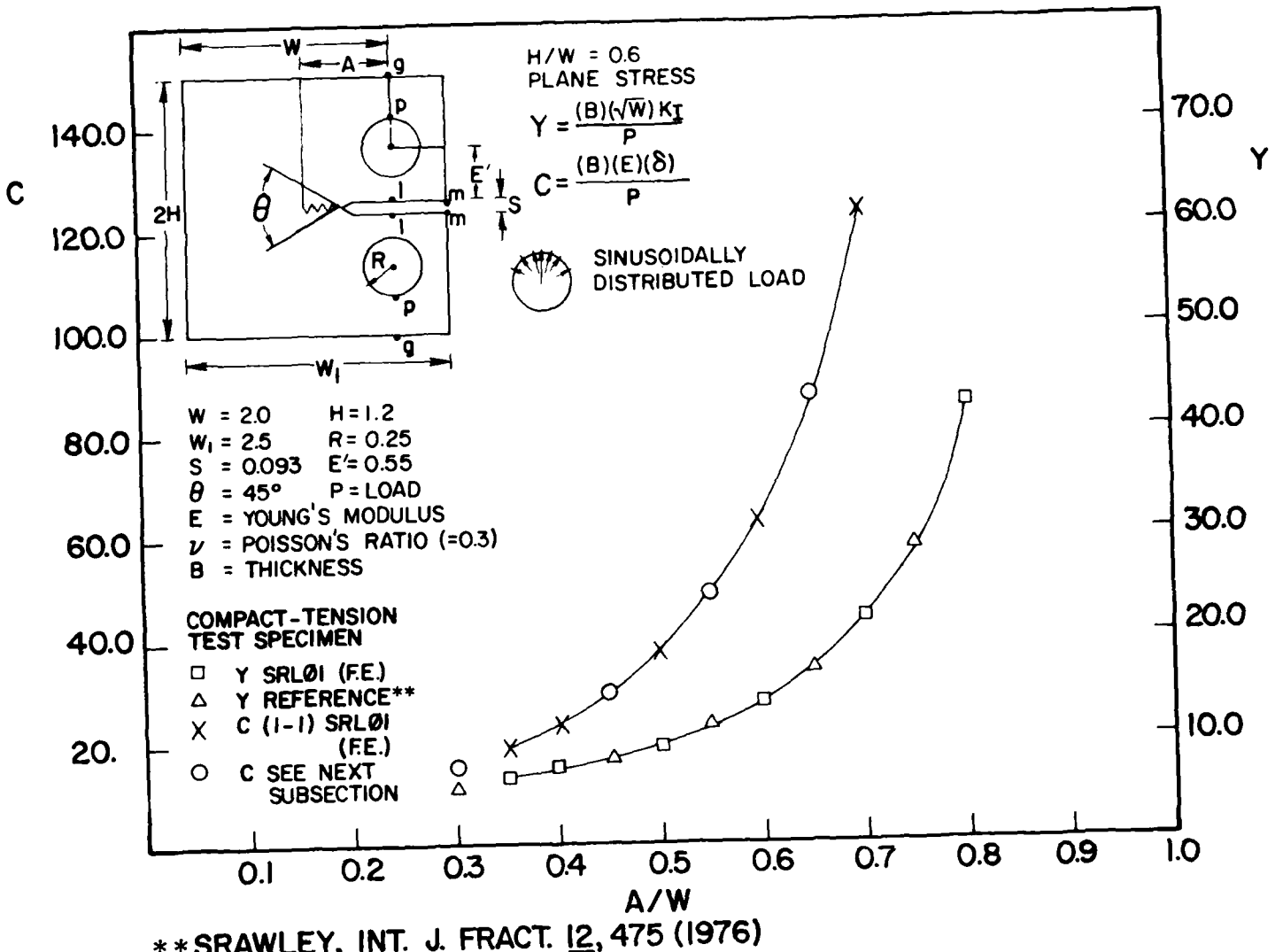


Figure 4. Analytical and Experimental Values of Nondimensional Compliance and Stress-Intensity Factor for CT Specimen Having Sinusoidally Distributed Pin Load

The geometric correction factor and ratios of various displacements to load for a compact-tension specimen shown in Tables VII and VIII were obtained to provide data necessary for experimental design purposes. The results show the effect of a sinusoidally distributed load at the hole (Table VII) as compared to a point load at the hole (Table VIII).

In Fig. 5 the results for a modified (H/W = 0.486) compact specimen are shown. This figure also provides a comparison of available experimental and analytical data and finite-element-analysis results. In Table IX some other potentially useful displacement values are given.

Analysis of a ring specimen was performed to provide analytical support for an experimental investigation. Figure 6 and Table X show the results of a single-notch ring specimen in compression. In Fig. 6, the compliance C is associated with the opening of the crack at the inner radius. The figure also gives a comparison with available results.

Due to anticipated experimental difficulties in loading the ring specimen under diametral compression, an analysis of the same specimen under diametrally opposed tensile loading was performed. The results show (Fig. 7) that the change in loading arrangement does not defeat the purpose (constant $K_I$ range) of using a ring specimen. Table XI contains some useful results for a single-notch ring specimen in tension.

b. Three-Dimensional Linear-Elastic Analysis

Development effort on a three-dimensional linear-elastic finite-element code has been completed. The program is based upon a twenty-noded distorted-brick-element formulation using Reissner's Variational Principle. A primary aim of the code after its evaluation is to analyze curved crack fronts.

TABLE VII

COMPACT SPECIMEN WITH SINUSOIDALLY DISTRIBUTED PIN LOAD

| | FINITE ELEMENT (SRLØ1) | | | | | | |
|---|---|---|---|---|---|---|---|
| A/W | Y | $\frac{C}{2}$ (m-m) | $\frac{C}{2}$ (l-l) | $\frac{C}{2}$ (p-p) | $\frac{C}{2}$ (q-q) | Y* | $\frac{C}{2}$** |
| 0.35 | 6.4046 | 14.54245 | 9.215694 | 10.34275 | 9.902922 | 6.39190 | 9.1376 |
| 0.4 | 7.2675 | 17.69912 | 11.60044 | 12.67651 | 12.23714 | 7.27873 | 11.4689 |
| 0.5 | 9.6407 | 26.96263 | 18.63661 | 19.68247 | 19.24289 | 9.65908 | 18.5423 |
| 0.6 | 13.7119 | 44.03555 | 31.76254 | 32.82077 | 32.38021 | 13.6541 | 31.8094 |
| 0.7 | 21.8700 | 82.08065 | 61.35191 | 62.43501 | 61.99355 | 21.5518 | 61.5715 |
| 0.8 | 42.4768 | 197.4746 | 1.51.9542 | 153.0611 | 152.619 | 41.1998 | 152.767 |

*Srawley, Int. J. Frac. 12, 475 (1976).

**See next subsection.



W = 2.0 H = 1.2
$W_1$ = 2.5 R = 0.25
S = 0.093 E' = 0.55
$\theta$ = 45° P = LOAD
E = YOUNG'S MODULUS
$\nu$ = POISSON'S RATIO (=0.3)
B = THICKNESS

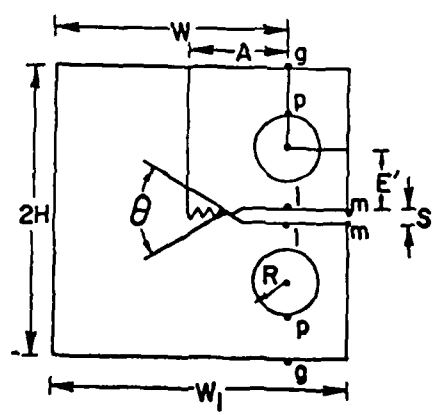


H/W = 0.6
PLANE STRESS

$$Y = \frac{B\sqrt{W}\,K_I}{P}$$

$$C = \frac{(B)(E)(\delta)}{P}$$

SINUSOIDALLY DISTRIBUTED LOAD

TABLE VIII

COMPACT SPECIMEN WITH CONCENTRATED PIN LOAD

| | FINITE ELEMENT (SRLØ1) | | | | | | |
|---|---|---|---|---|---|---|---|
| A/W | Y | $\frac{C}{2}$ (m-m) | $\frac{C}{2}$ (1-1) | $\frac{C}{2}$ (p-p) | $\frac{C}{2}$ (q-q) | Y* | $\frac{C}{2}$** |
| 0.35 | 6.37451 | 14.55624 | 8.891305 | 11.65514 | 10.33469 | 6.39190 | 9.1376 |
| 0.4 | 7.25637 | 17.70461 | 11.26977 | 13.98276 | 12.66276 | 7.27873 | 11.4689 |
| 0.5 | 9.64482 | 26.96656 | 18.30516 | 20.98765 | 19.66750 | 9.65908 | 18.5423 |
| 0.6 | 13.71740 | 44.04669 | 31.43724 | 34.13143 | 32.81030 | 13.6541 | 31.8094 |
| 0.7 | 21.87322 | 82.09984 | 61.03389 | 63.75179 | 62.42976 | 21.5518 | 61.5715 |
| 0.8 | 42.47798 | 197.4998 | 151.6423 | 154.3823 | 153.0596 | 41.1998 | 152.767 |

*Srawley, Int. J. Frac. 12, 475 (1976).

**See next subsection.

W = 2.0 H = 1.2
$W_1$ = 2.5 R = 0.25
S = 0.093 E' = 0.55
$\theta$ = 45° P = LOAD
E = YOUNG'S MODULUS
$\nu$ = POISSON'S RATIO (=0.3)
B = THICKNESS

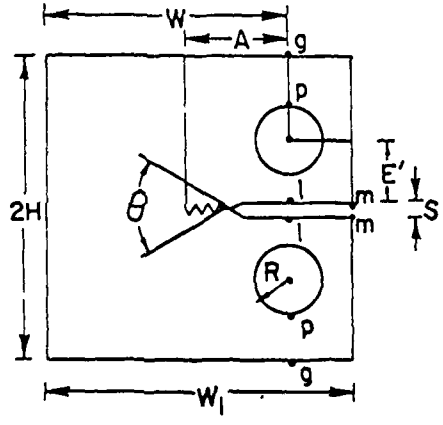


H/W = 0.6
PLANE STRESS

$$Y = \frac{(B)(\sqrt{W})K_I}{P}$$

$$C = \frac{(B)(E)(\delta)}{P}$$

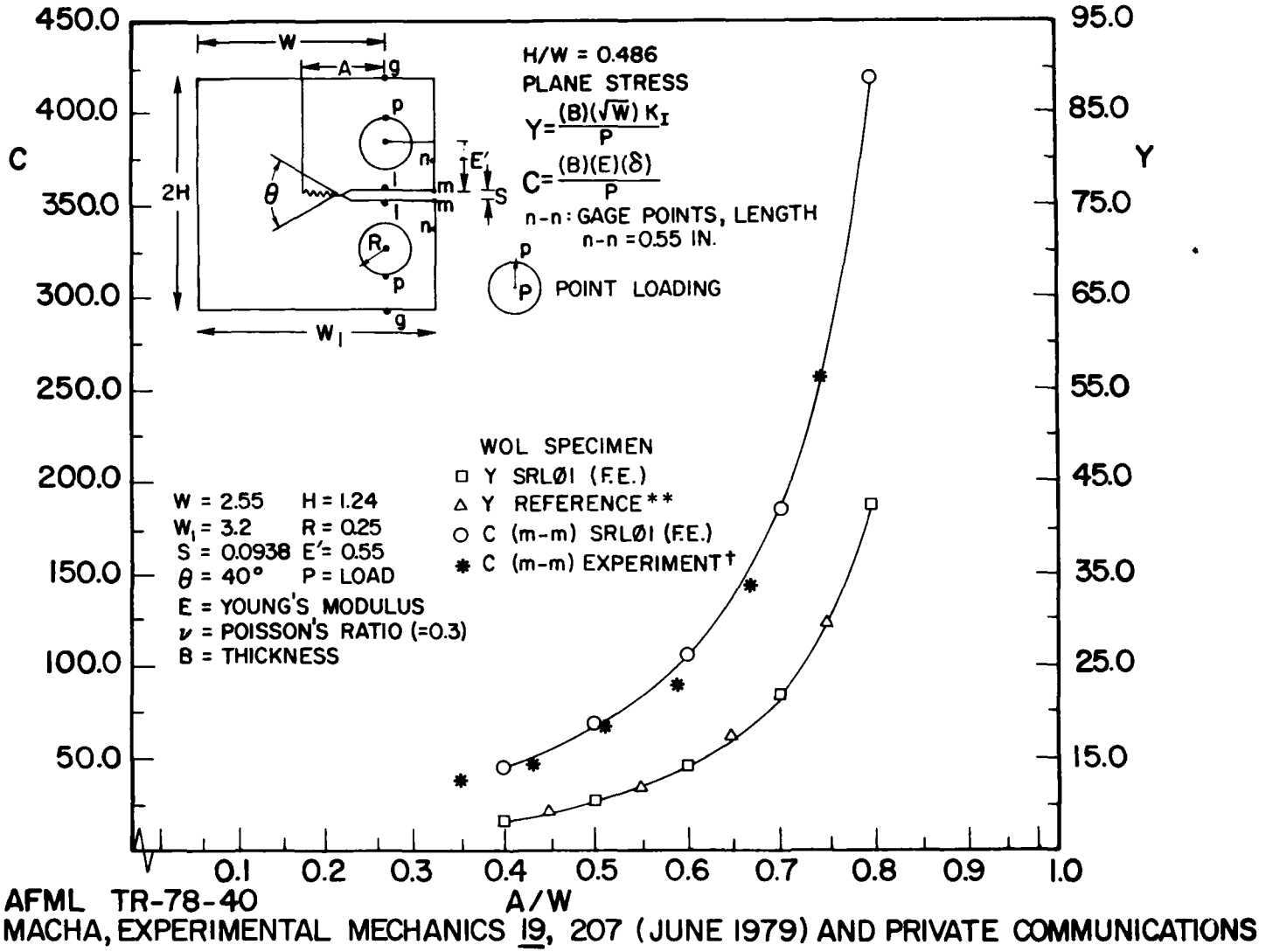


**AFML TR-78-40

† MACHA, EXPERIMENTAL MECHANICS 19, 207 (JUNE 1979) AND PRIVATE COMMUNICATIONS

Figure 5. Analytical and Experimental Value of Nondimensional Compliance and Stress-Intensity Factor for WOL Specimen with Concentrated Pin Loads

TABLE IX

MODIFIED COMPACT SPECIMEN

| FINITE ELEMENT (SRLØ1) | | | | | | REFERENCE* | | | SRLØ1 | EXP. RESULTS** |
|---|---|---|---|---|---|---|---|---|---|---|
| A/W | Y | C (m-m) | C (1-1) | $\frac{C}{2}$ (p-p) | $\frac{C}{2}$ (g-g) | Y | C (1-1) | C (m-m) | C (n-n) | C (m-m) |
| 0.352 | --- | --- | --- | --- | --- | --- | --- | --- | --- | 39.683 |
| 0.4 | 8.1265 | 44.25632 | 27.9493 | 16.53571 | 15.17502 | 8.1401 | 28.545196 | 45.239419 | 44.18088 | --- |
| 0.431 | --- | --- | --- | --- | --- | --- | --- | --- | --- | 45.605 |
| 0.5 | 10.3311 | 67.1919 | 45.11700 | 25.02486 | 23.66484 | 10.3012 | 45.3338156 | 67.776923 | 67.11888 | --- |
| 0.509 | --- | --- | --- | --- | --- | --- | --- | --- | --- | 67.021 |
| 0.588 | --- | --- | --- | --- | --- | --- | --- | --- | --- | 91.827 |
| 0.6 | 14.1225 | 105.15126 | 74.0288 | 39.50525 | 38.1442 | 14.0448 | 74.2425721 | 106.168544 | 105.07736 | --- |
| 0.668 | --- | --- | --- | --- | --- | --- | --- | --- | --- | 144.961 |
| 0.7 | 21.9323 | 184.3378 | 135.2912 | 70.15431 | 68.79270 | 21.7924 | 135.823680 | 184.87858 | 184.26346 | --- |
| 0.747 | --- | --- | --- | --- | --- | --- | --- | --- | --- | 257.671 |
| 0.8 | 42.1373 | 417.0342 | 317.2428 | 161.1404 | 159.7786 | 41.3462 | 320.568894 | 414.919617 | 416.9592 | --- |

*AFML TR-78-40.

**See Macha reference on Fig. 5.

W = 2.55 H = 1.24
$W_1$ = 3.2 R = 0.25
S = 0.0938 E' = 0.55
$\theta$ = 40° P = LOAD
E = YOUNG'S MODULUS
$\nu$ = POISSON'S RATIO (=0.3)
B = THICKNESS

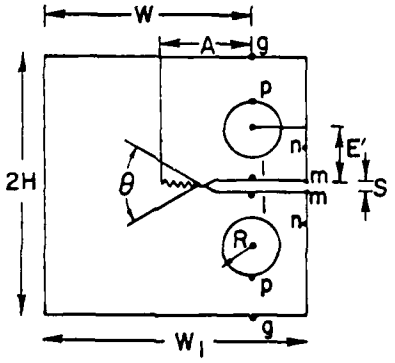


H/W = 0.486
PLANE STRESS

$$Y = \frac{(B)(\sqrt{W})\,K_I}{P}$$

$$C = \frac{(B)(E)(\delta)}{P}$$

n-n: GAGE POINTS, LENGTH
n-n = 0.55 IN.

POINT LOADING

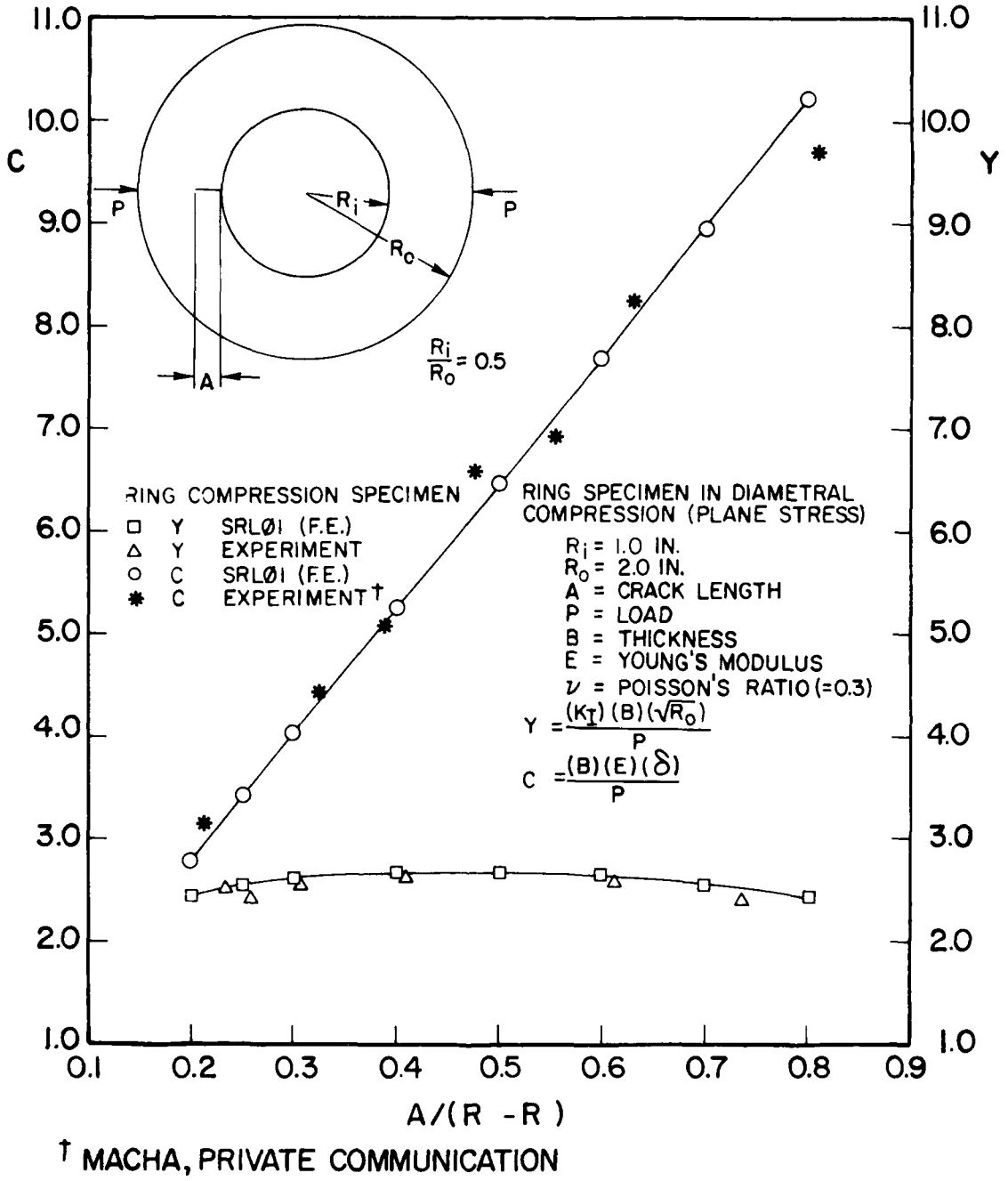


Figure 6. Analytical and Experimental Value of Nondimensional Compliance and Stress-Intensity Factor for Ring Specimen Under Compressive Loads, $R_i/R_o$ = 0.5

TABLE X

RING COMPRESSION SPECIMEN

| FINITE ELEMENT (SRLØ1) | | | | EXPERIMENT | |
|---|---|---|---|---|---|
| $A/(R_o-R_i)$ | Y | C (m-m) | C (1-1) | Y* | C** |
| 0.2 | 2.44659 | 2.79049 | 13.20882 | - | - |
| 0.217 | - | - | - | - | 3.205118 |
| 0.25 | 2.54558 | 3.42292 | 13.55158 | - | - |
| 0.236 | - | - | - | 2.500 | - |
| 0.258 | - | - | - | 2.375 | - |
| 0.3 | 2.61771 | 4.03712 | 13.88358 | - | - |
| 0.306 | - | - | - | 2.52 | - |
| 0.327 | - | - | - | - | 4.427822 |
| 0.388 | - | - | - | - | 5.02952 |
| 0.4 | 2.67286 | 5.24546 | 14.57081 | - | - |
| 0.412 | - | - | - | 2.63 | - |
| 0.474 | - | - | - | - | 6.55939 |
| 0.5 | 2.67852 | 6.45932 | 15.31517 | - | - |
| 0.518 | - | - | - | 2.75 | - |
| 0.553 | - | - | - | - | 6.96245 |
| 0.576 | - | - | - | 2.63 | - |
| 0.6 | 2.61629 | 7.69610 | 16.07635 | - | - |
| 0.612 | - | - | - | 2.420 | - |
| 0.633 | - | - | - | - | - |
| 0.7 | 2.54063 | 8.96066 | 16.73128 | - | - |
| 0.734 | - | - | - | 2.270 | - |
| 0.738 | - | - | - | - | 9.156496 |
| 0.8 | 2.41136 | 10.21596 | 17.16722 | - | - |
| 0.805 | - | - | - | - | 9.71456 |

*Jones, Engrg. Frac. Mech. 6, 435 (1974).

**Macha, Private Communication.

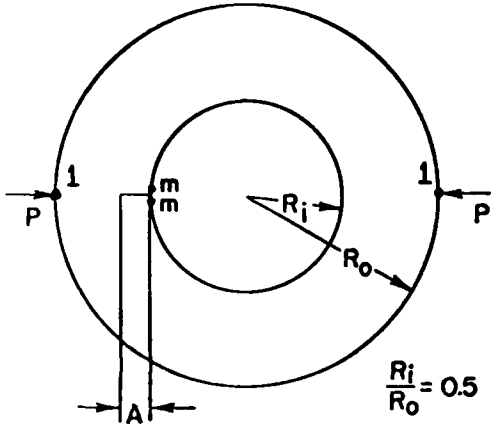


RING SPECIMEN IN DIAMETRAL COMPRESSION (PLANE STRESS)

$R_i$ = 1.0 IN.
$R_o$ = 2.0 IN.
A = CRACK LENGTH
P = LOAD
B = THICKNESS
E = YOUNG'S MODULUS
$\nu$ = POISSON'S RATIO (=0.3)

$$Y = \frac{(K_I)(B)(\sqrt{R_o})}{P}$$

$$C = \frac{(B)(E)(\delta)}{P}$$

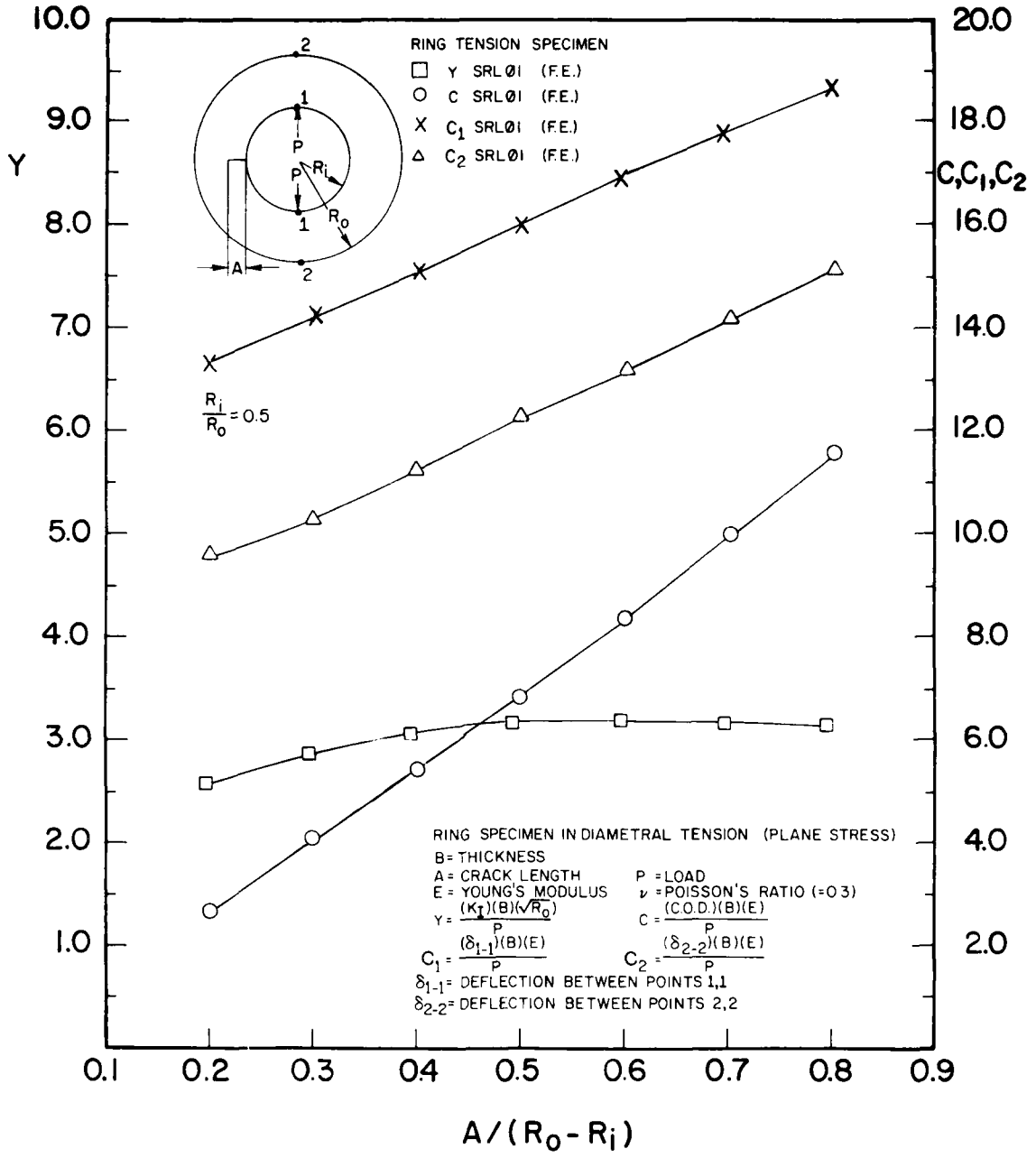


Figure 7. Analytical and Experimental Value of Nondimensional Compliance and Stress-Intensity Factor for Ring Specimen Under Tensile Loads, $R_i/R_o = 0.5$

TABLE XI

RING TENSION SPECIMEN

FINITE ELEMENT (SRLØ1) RESULTS

| $A/(R_o-R_i)$ | Y | $\frac{C\ (m-m)}{2}$ | $\frac{C_1\ (1-1)}{2}$ | $\frac{C_2\ (2-2)}{2}$ |
|---|---|---|---|---|
| 0.2 | 2.59882 | 1.388955 | 6.752161 | 4.813811 |
| 0.3 | 2.88839 | 2.057702 | 7.12705 | 5.197950 |
| 0.4 | 3.05609 | 2.739379 | 7.547198 | 5.631572 |
| 0.5 | 3.15695 | 3.452466 | 7.997314 | 6.097367 |
| 0.6 | 3.20632 | 4.202697 | 8.464212 | 6.581717 |
| 0.7 | 3.22062 | 4.989064 | 8.935710 | 7.073110 |
| 0.8 | 3.19440 | 5.786337 | 9.385786 | 7.544692 |

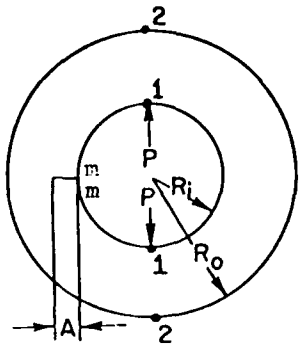


$\frac{R_i}{R_o} = 0.5$

RING SPECIMEN IN DIAMETRAL TENSION (PLANE STRESS)

B = THICKNESS

A = CRACK LENGTH  P = LOAD

E = YOUNG'S MODULUS  $\nu$ = POISSON'S RATIO (=0.3)

$Y = \frac{(K_I)(B)(\sqrt{R_o})}{P}$  $C = \frac{(C.O.D.)(B)(E)}{P}$

$C_1 = \frac{(\delta_{1-1})(B)(E)}{P}$  $C_2 = \frac{(\delta_{2-2})(B)(E)}{P}$

$\delta_{1-1}$ = DEFLECTION BETWEEN POINTS 1,1

$\delta_{2-2}$ = DEFLECTION BETWEEN POINTS 2,2

c. Two-Dimensional Elastic-Plastic Analysis

Development of a computer code for two-dimensional viscoplastic analysis was initiated. The salient features of the program are

1. Treatment of time-dependent plasticity.

2. Adaptability of a wide range of available plasticity potentials (von Mises, Tresca, Bodner, etc.).

## 5. ANALYSIS OF CRACK SPECIMENS USING COMPLIANCE CONCEPTS

Since some degree of success has been achieved in the application of stress-intensity factors in correlating crack-growth behavior in engine materials under operating conditions, an associated analysis of displacements of the material containing a crack or flaw should also be applicable. Possible uses of the analysis of displacements include the resolution of phenomena such as crack closure and fatigue-crack retardation. The term compliance is defined as the ratio of a displacement in a specified direction to an applied load on the specimen. For linear-elastic fracture mechanics which provides the theoretical framework for the stress-intensity factors, the compliance for a particular displacement of the specimen is a constant, i.e., independent of the value of the load.

Generally, the compliance is a function of the geometry which includes the crack length of the specimen and the location of the applied loads on the specimen. As a result of this functional relationship, the analytical results for compliance have applications in the laboratory for conducting continuously operating tests, automating the evaluation of crack lengths, determining an effective crack length, and evaluating a test set-up.

The first application would allow the test machine to be used twenty-four hours a day, which would provide more efficient use of the machine. The crack could be determined without periodically stopping the test to

make an optical measurement of the length. Allowing continuous test operation becomes a necessity when investigating the interaction between a time-dependent environmental phenomena and cyclic crack-growth rate. The second application would avoid the need for a technician to make periodic crack-length measurements on a specimen. The third application can be used when extensive curvature of the crack front develops and, thus, surface crack-length measurements do not provide a direct correlation with the crack-growth behavior.

Once confidence is established for the use of compliance measurements, a deviation from the expected result for a known geometry could indicate an incorrect test set-up. For example, if a loading pin should stick in a specimen, an internal bending moment would develop but would not be indicated on the load cell of the test frame. However, the moment would cause an additional deflection which would alter the expected compliance value.

In order to conduct this study which would provide a fundamental understanding for future applications in the laboratory, an accurate method of analysis of the various specimen geometries was needed. Two theoretical methods have been developed partially under this program which provide readily available computer programs and expertise to facilitate their use. These methods of analysis were based upon the boundary integral equation (BIE)[3] and the finite-element (FE) (see subsection on pp. 50-61 of this report) formulations of fracture-mechanics problems. Both formulations lent themselves to the compliance study because displacements could be conveniently calculated at points on the body where measurements were made and various loading conditions could be introduced into the analysis.

A comparison of the results from the BIE and FE formulations for a CT specimen is shown in Fig. 8 for the compliances associated with the following points (see inset of Fig. 8):

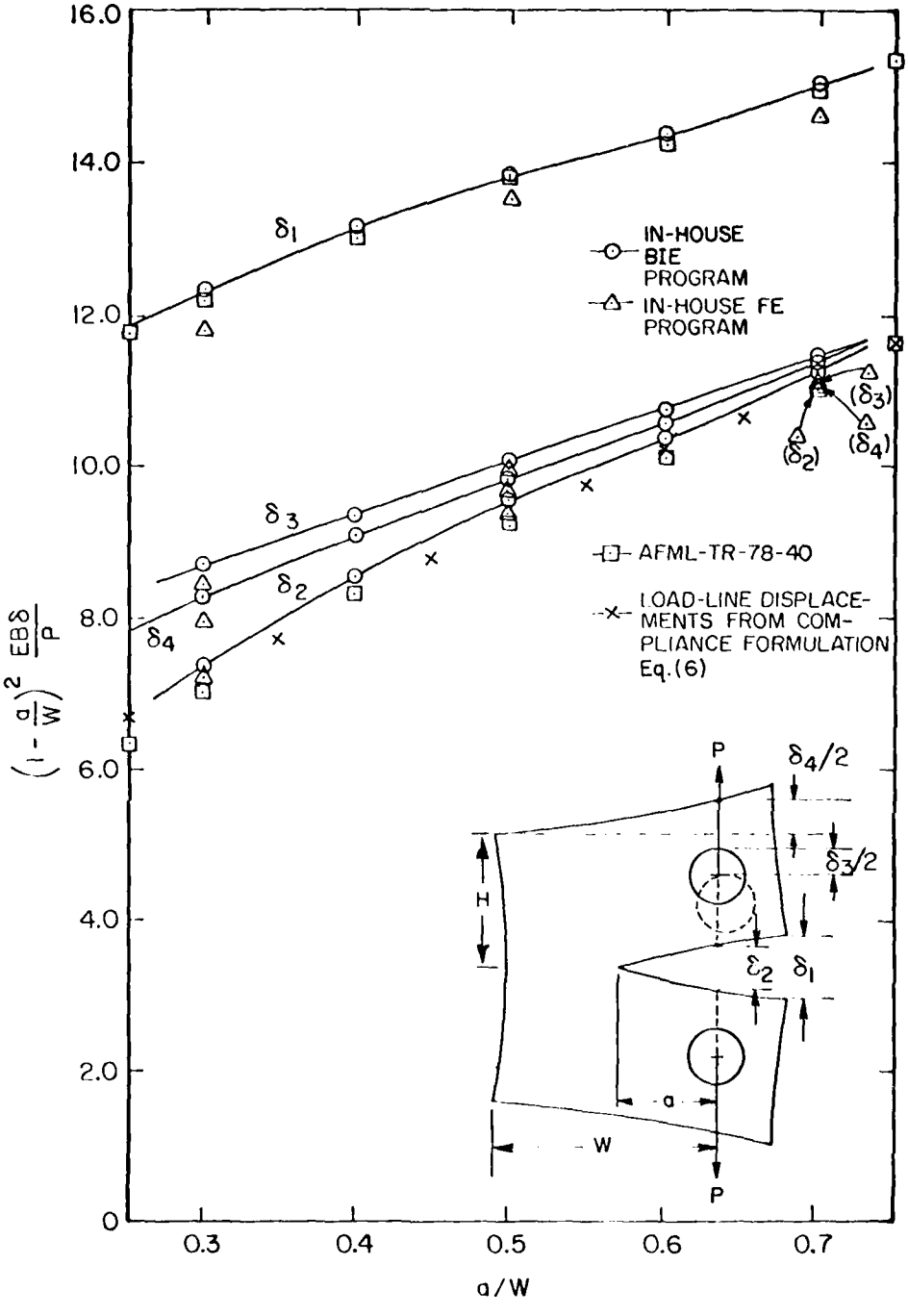


Figure 8. Analytical Results of Various Compliance Values, $\delta/P$, for a CT Specimen

at the notch surfaces along the load-line, $\delta_1$

at the notch surfaces at the edge of the specimen, $\delta_2$

at the loading pins, $\delta_3$

at the top and bottom surfaces along the load-line, $\delta_4$

The results in Fig. 8 for compliance which is given by the ratio $\delta/P$ are applicable to any material with Young's modulus, E, and thickness, B.

There is fairly good agreement between the two methods. In addition, these results were compared to available results which in the literature were typified by Ref. 7 and also which were obtained by integration of the commonly known theoretical relationship between a compliance, $\bar{C}$, for plane-stress deformation problems and the stress-intensity factor, K,

$$K^2 = \frac{1}{2} E \frac{P^2}{B} \frac{\partial \bar{C}}{\delta a} , \qquad (6)$$

where P is the load. Integration of (6) when K is given by the expression for CT or three-point-bend specimens in Ref. 8 yields a compliance which is associated with the load-line displacement of point loads or equivalently, with the work done by loads on the body. Results of the integration are plotted in Fig. 8 and in Fig. 3 as the triangular points. While this type of compliance is of theoretical and practical interest, it is difficult to measure in the CT specimen. Therefore, other points in the specimen are used to measure displacements which are equivalent to the load-line displacement. Such conveniently measured displacements are $\delta_2$ and $\delta_4$. Indeed, the results of $\delta_4$ from the BIE analysis were critical in the design of the experimental set-up for crack-growth under sustained load (see subsection on pp. 11-15 of this report).

With the proven capability to provide accurate theoretical results, data were collected on compliance in order to assess the capabilities of the instrumentation and the potential of the experimental set-up. In order to determine crack length from compliance measurements for the elevated-temperature fatigue-crack-growth tests, an extensometer was designed to be used for conjunction with the resistance furnace.

Based upon the experience gained from the development of the LCF extensometer, the design of the extensometer for the resistance furnace incorporated adaptors for the arms of an MTS Model 632.11B-20 clip gage. The adaptors hold the quartz rods with V-shaped ends which are pulled into notches on the edge of a specimen by springs. A resistance furnace was modified to accept the quartz rods and spring attachments. Preliminary tests using this extensometer on an Al CT specimen have been initiated and the data indicate that the extensometer design and attachment provide accurate and reliable measurements.

To supplement the investigation of compliance for fatigue-crack growth at elevated temperatures, other compliance data which were obtained in the laboratory from other types of tests have been compared in Fig. 9 to the analytical results. The nondimensional values, $E\overline{BC}$, of some of these compliances are given in Table XII. These values for the compact-type specimen were collected for various materials--304 stainless steel which was discussed in the subsection on pp. 11-12 of this report, an aluminum alloy which was used for some preliminary tests on the elevated-temperature fatigue-crack extensometer, and four materials which were tested in the corrosion-inhibitor task of this program--and for various thicknesses. The nondimensional experimental values compare very favorbly with the analytical results given in Fig. 9. This agreement supports the general application of the analytical results to various types of material response characterized by Young's modulus and to various values for the thickness and width of the standard compact specimen.

For the corrosion task the crack-opening displacement, COD or equivalently $\delta_1$ in Fig. 9, and the surface crack length were measured for each size

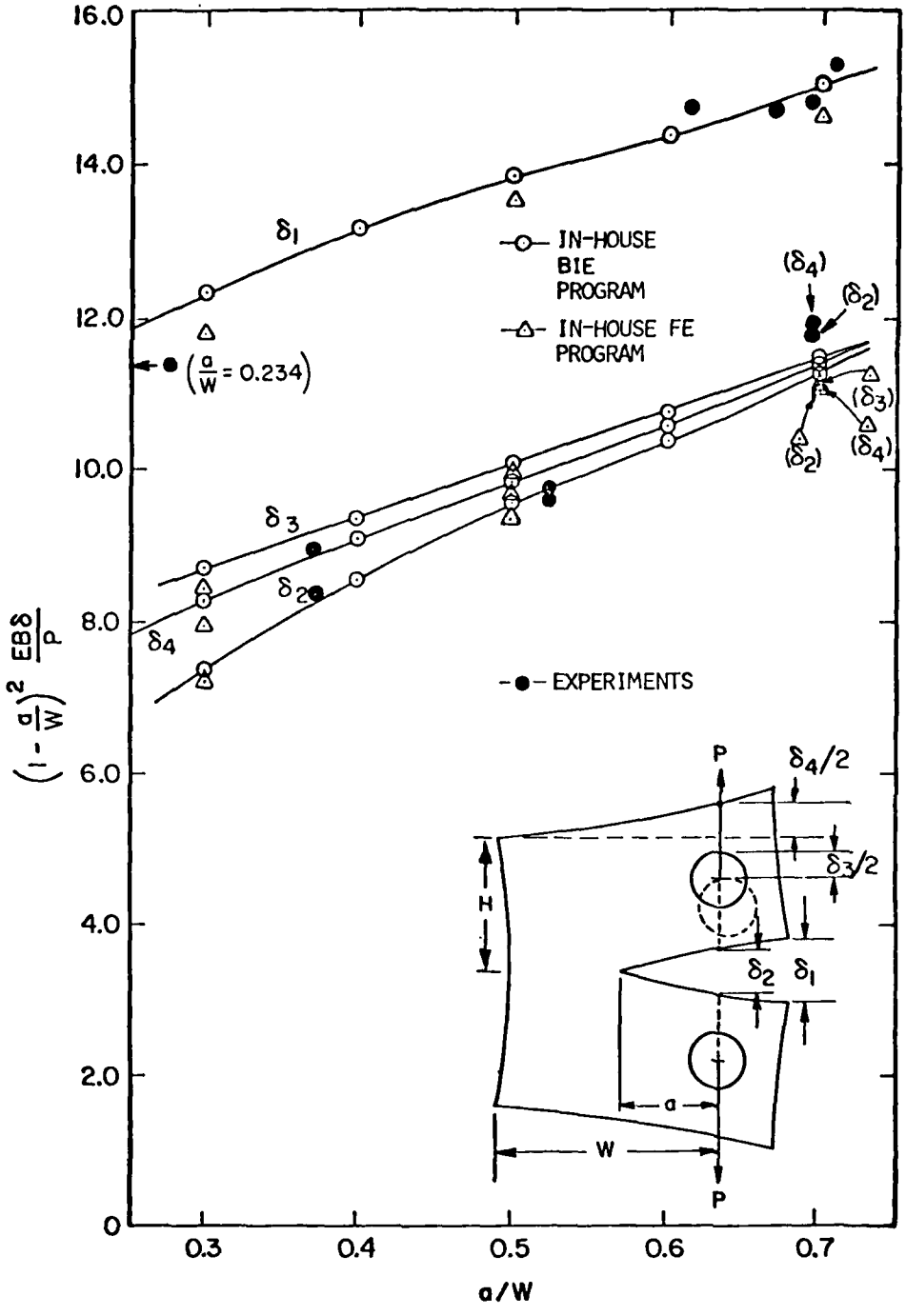


Figure 9. Analytical and Experimental Displacements in a Compact Specimen

TABLE XII

VARIOUS EXPERIMENTAL COMPLIANCE MEASUREMENTS

(Room temperature unless otherwise noted)

| Material | Geometry | Displ. Meas.[a] | E ($10^6$ psi) | B (in.) | W (in.) | a/W (-) | $EB\bar{C}$ (-) | $(1-a/W)^2 \times EB\bar{C}$ (-) |
|---|---|---|---|---|---|---|---|---|
| 304 Stainless Steel | CT | $\delta_4$ | 29. | 0.5 | 2.00 | 0.39 | 22.8 | 8.48 |
| | | " | " | " | " | 0.54 | 41.9 | 8.87 |
| | | " | " | " | " | 0.71 | 144. | 12.1 |
| | | $\delta_2$ | " | " | " | 0.39 | 21.4 | 7.96 |
| | | " | " | " | " | 0.54 | 41.6 | 8.80 |
| | | " | " | " | " | 0.71 | 142. | 11.9 |
| Aluminum Alloy | CT | $\delta_1$[c] | 10.5 | 0.25 | 2.00 | 0.234 | 19.7 | 11.4 |
| IN 100[b] | CT | $\delta_4$ | 25.2 | 0.469 | 2.00 | 0.70 | 18.9 | 8.0 |
| PM Aluminum Alloy | CT | $\delta_1$ | 10. | 1.05 | 2.00 | 0.65 | 119. | 14.6[d] |
| Hi-Strength Aluminum Alloy | CT | " | 10.5 | 1.00 | 2.00 | " | 120. | 14.7[d] |
| Mod. HY 180 Steel | CT | " | 29. | 0.9 | 18.28 | " | 122. | 15.0[d] |
| Hi-Strength Steel Alloys | CT | " | 30. | 0.75 | 1.50 | " | 114. | 14.0[d] |
| Polycarbonate | Three-Point Bend | $\delta_{LL}$[e] | 0.325 | 0.994 | 1.0 | 0.256 | 25.5 | 14.1 |
| | | | " | " | " | 0.352 | 32.1 | 13.4 |
| | | | " | " | " | 0.438 | 41.5 | 13.1 |

[a] Refer to insert of Fig. 9 for displacement-measurement points.

[b] Test temperature of 732°C (1350°F).

[c] Measurement points slightly above and below those indicated on Fig. 9.

[d] Results taken from polynomial fit to data.

[e] Displacement of the load on the middle of the beam along the load-line.

of compact test specimen. The compliance was computed from the ratio of the change in COD ($\Delta$COD) to the change in load ($\Delta$P) for various crack lengths. The coefficients of a polynomial for each of the four materials were determined such that a least-squares fit was obtained for the compliance-vs-crack length data. Values computed from these four polynomial are plotted in Fig. 10 along with the analytical results. In terms of the nondimensional variables for Fig. 10, a correlation does exist amoung the four polynomials and the analytical results for a/W in the approximate range of 0.6 to 0.7, which was the range of the experimental data. However, the results from one specimen cannot adequately yield the correct calibration between compliance and crack length. As expected from such a least-squares polynomial fit to experimental data, an extrapolation outside the range of data would generally produce an incorrect result. Thus, the analytical results provide a better and broader understanding of the dependence of compliance upon crack length than can be produced by the experimental data.

Compliance values have also been obtained for ring specimens (see previous section). However, data were not available for a variety of material moduli and dimensions. The experimentally determined compliances listed in Table XII have been compared to the analytical results in Figs. 3 and 9. Again, agreement between the experiment and the analysis is very good.

a. Reduction of Fatigue-Crack-Length Data

In modeling and characterizing fatigue-crack-growth behavior of materials, collection and reduction of experimental data are necessary in order to obtain basic information on crack-growth rates and stress-intensity factors. A computer program to reduce experimental fatigue-crack length and cycle-count data which were obtained under constant-load amplitude tests was available in the laboratory. The program was written to reduce data obtained for standard compact specimens. The data reduction produced cyclic crack-growth rates and stress-intensity factors based upon a five-point movable strip analysis. In this analysis the coefficients

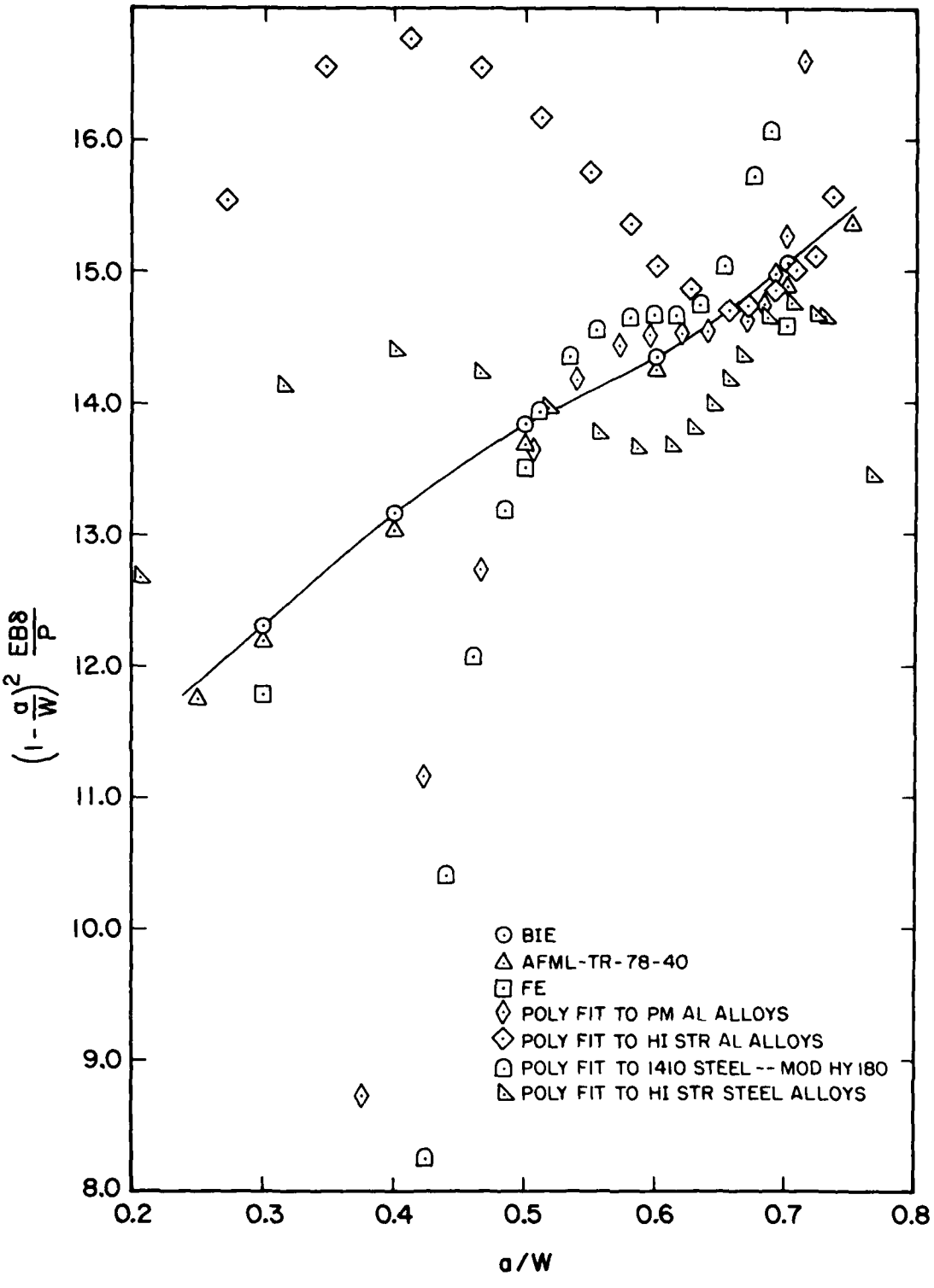


Figure 10. Comparison of Results from Polynomial Fits to Experimentally Derived Compliances and Analytical Results for Compliances of Compact Specimens

of a second-degree polynomial were determined to obtain a least-squares fit to five consecutive data points for crack length and cycle count. From the polynomial fit, the values of crack length and cyclic crack-growth rate or slope were compu_ed at the middle of the range of the five cycle counts. The value of the crack length was used to compute the stress-intensity factor. Then the procedure was repeated for the next set of five data points which was formed by removing the first data point in the previous set and adding the next successive data point. The data-reduction technique provides a relative smoothing of the resolved data which is required because the inherent scatter in the raw data is generally magnified during a differentiation process. The computer program also computed the crack length and slope at the beginning value and the first quarter point in the range of the first set of five cycle counts and at the last value and the third quarter point in the range of the last set of five cycle counts. Thus, the number of reduced data points was equal to the number of raw data points.

Under this task the computer program was generalized to reduce the following types of data in addition to crack-length and cycle-count data:

Crack length and time data.
Compliance and cycle-count or time data.
Displacement and cycle-count or time data.

for the following, common laboratory specimens in addition to the standard compact specimen:

Modified compact specimen (H/W = 0.486).
Single-edge notch specimen.
Center-cracked specimen.
Three-point bend specimen (S/W = 4.).

In an application of the original program to a set of data, irregular results were obtained which were ultimately traced to a numerical instability when the least-squares polynomial fit was determined. This instability was eliminated by translating the cycle-count values before the least-squares calculations were made.

Other modifications provided the capability to reduce data from variable-amplitude load conditions which occurred in experiments where load shedding was employed. Also, instead of evaluating the crack length and slope at the middle of the range of cycle counts, the crack length and slope were computed at the third cycle-count value in each five-point set of data and at the first and second cycle counts in the first five-point set and at the next-to-last and last cycle counts in the last five-point set.

ASTM has adopted a tentative test method for obtaining fatigue-crack-growth rates and recommended acceptable data-reduction techniques.[9] Essentially, the techniques suggested in the method have been incorporated in the modified computer program. The ASTM method did not recommend that a specific number of data points be used for the polynomial fit but suggested that either three, five, seven, or nine points could be used. The program was modified to permit the user to select any odd number from three (3) to twenty-one (21) data points for the polynomial fit.

An analysis was conducted on data obtained from a corrosion-fatigue crack-growth experiment. Corrosion-fatigue data were selected because they have a higher degree of scatter than fatigue-crack-growth data. A plot of the data for crack length vs. cyclic count is shown in Fig. 11. The values of crack length were obtained from COD measurements and an experimentally determined calibration curve between crack length and COD as shown in Fig. 10.

Using three, eleven, and fifteen for the number of data points in the movable strip, the reduction technique yielded the results for crack-growth rate and range of the stress-intensity factor which are shown in Figs. 12, 13, and 14, respectively. It should be noted that the jump in crack-growth rate which occurred before the last two data

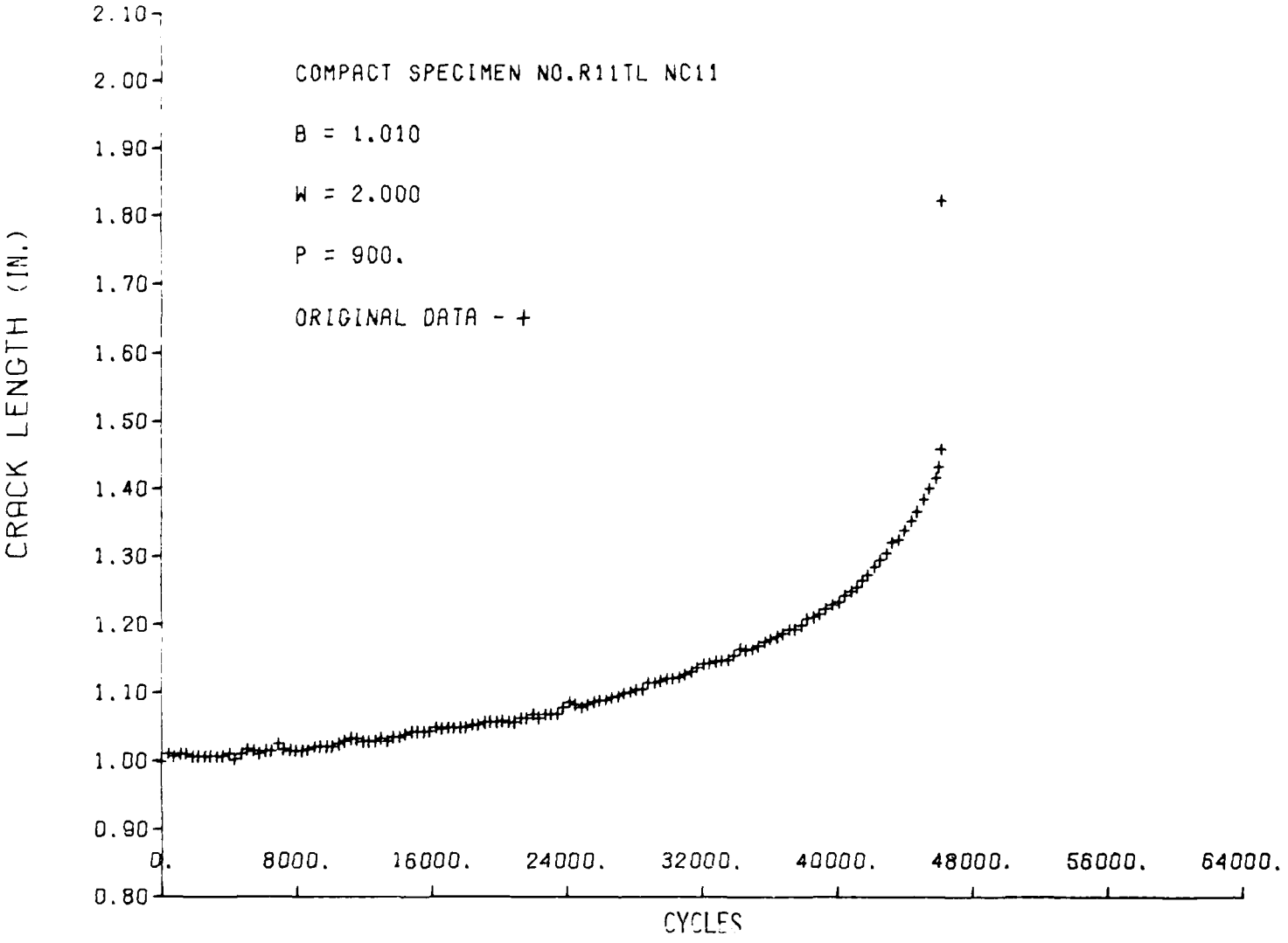


Figure 11. Plot of Crack Length as a Function of Cycles for a Corrosion-Fatigue Crack-Growth Test

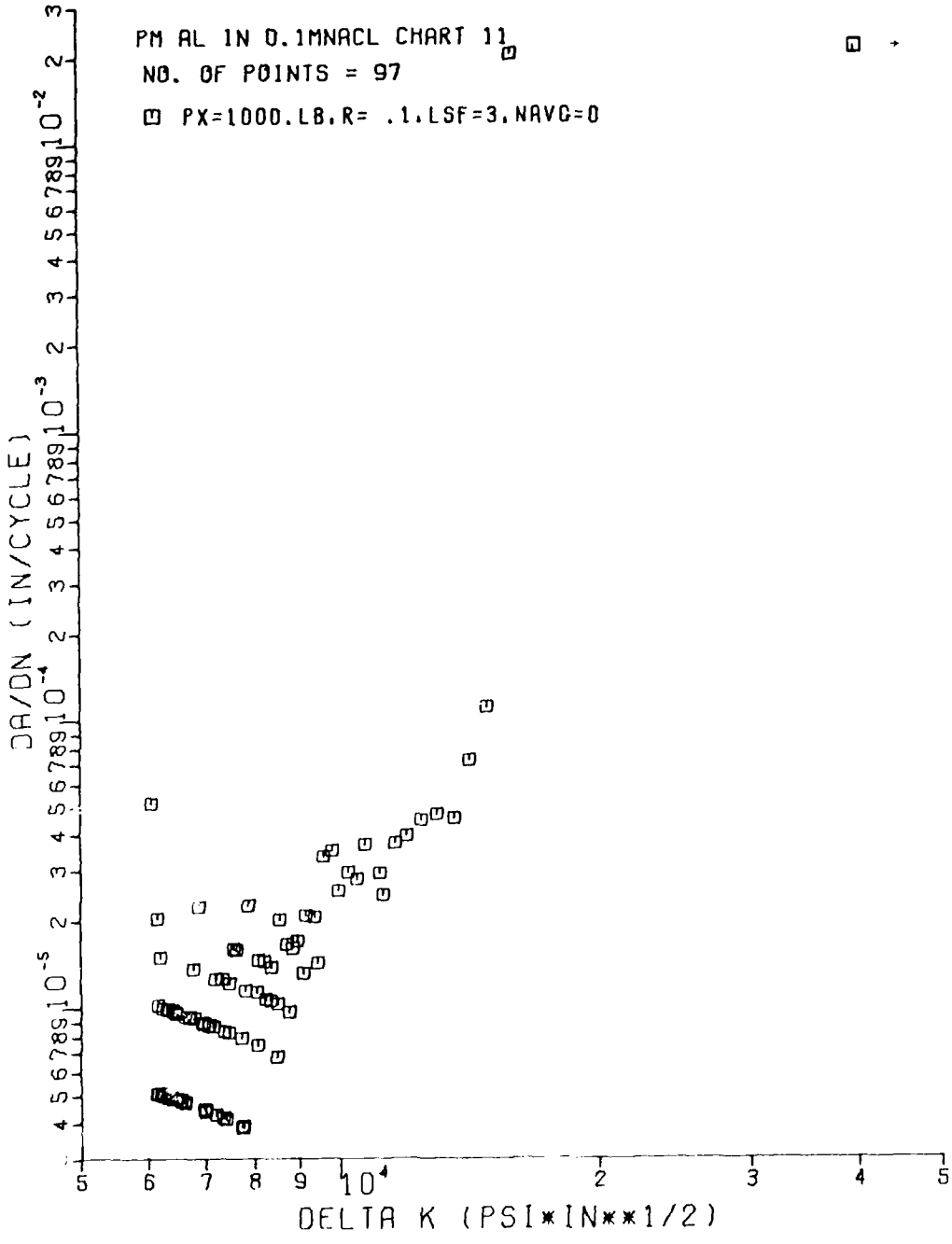


Figure 12. Crack-Growth Rate Obtained from Data on Fig. 11 by Use of a Least-Squares Fit to Three Successive Data Points

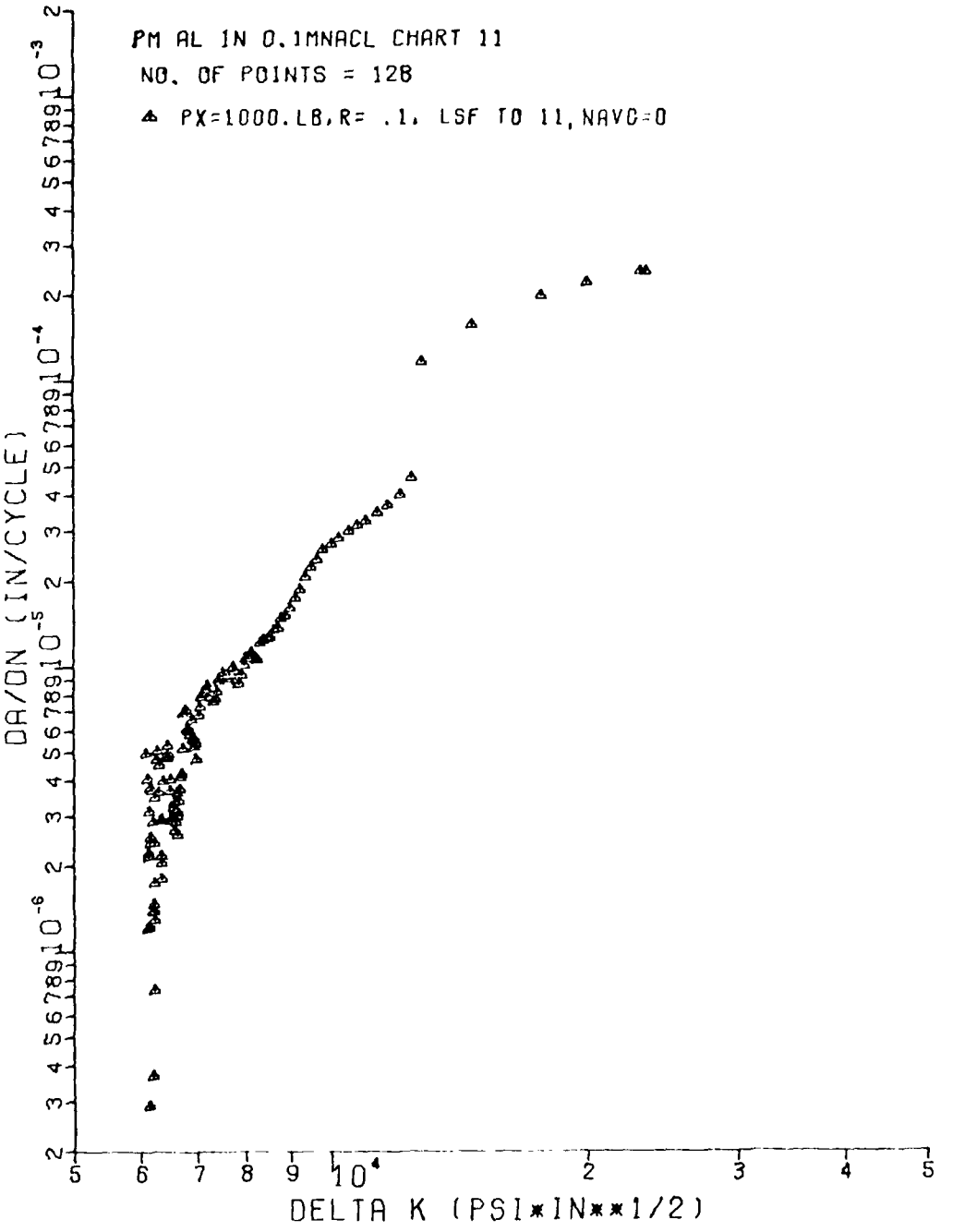


Figure 13. Crack-Growth Rate Obtained from Data on Fig. 11 by Use of a Least-Squares Fit to Eleven Successive Data Points

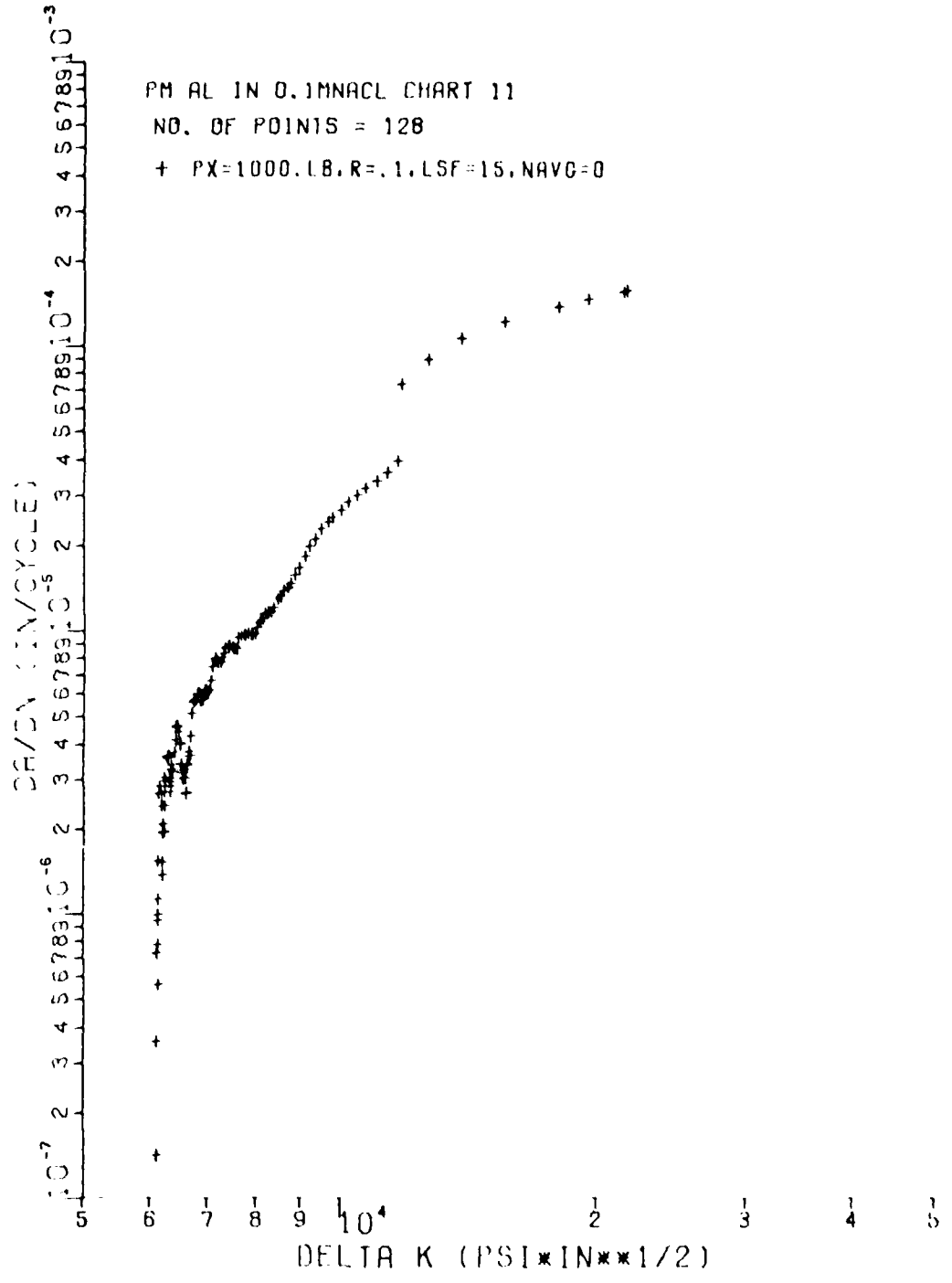


Figure 14. Crack-Growth Rate Obtained from Data on Fig. 11 by Use of a Least-Squares Fit to Fifteen Successive Data Points

points at the top of Fig. 12, the last six data points in Fig. 13, and the last eight data points in Fig. 14 was due to the last crack-length value in Fig. 11 which was determined by an extrapolation of the calibration curve. As discussed earlier, an experimentally determined calibration curve will generally produce errors when applied outside the range of the original data.

The results in Figs. 12-14 illustrate that the reduced data have been smoothed by selecting a larger number of data points for the least-squares fit. Also, a larger amount of data--97 data points as compared to 128 points--has been resolved by using eleven or fifteen data points instead of three. Since the reduced data were not biased by selecting larger numbers of points, the trends of the data have been clarified. Having a variable number of points in the data-reduction method allows the user to accurately resolve a set of data having a large amount of scatter.

b. Microstructural Observation of IN-100 (Gatorized) Subjected to Sustained-Load Tests

Standard test specimens of designations 7-1, 11-2, 23-1, and 15-1 fractured during tests at 732°C (1350°F) [in the case of #15-1, the specimen was accidentally overheated to 843°C (1550°F)] were observed for evaluation of the fracture-mode using a scanning electron microscope. Visual observation of the fracture surfaces indicated dramatic changes in the fracture appearance from the edge to the center of the specimens; the fracture appearance at the edge of the specimen was smooth and at the center of the specimen was very rough and jagged with ridges and valleys extending along the length of the specimen (Fig. 15 shows a typical scanning electron micrograph taken at 25× from Specimen #7-1). However, when the fracture surfaces were observed in detail at higher magnifications in the SEM, the fractographs appeared to be similar in the edge and in the central region of the specimens. (Figure 16 is a typical scanning electron micrograph from Specimen #7-1.)

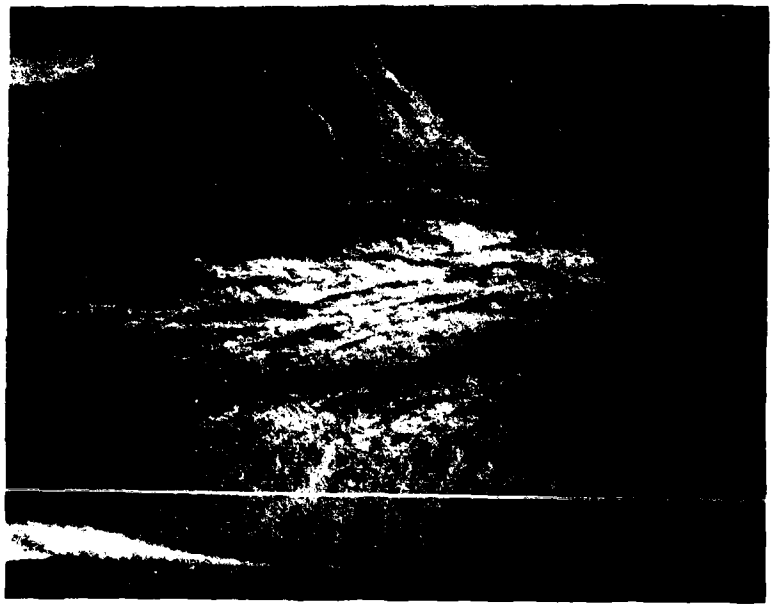

Figure 15. Micrograph of Fracture Surface of IN 100 (Gatorized) Formed Under Constant Load (25×)

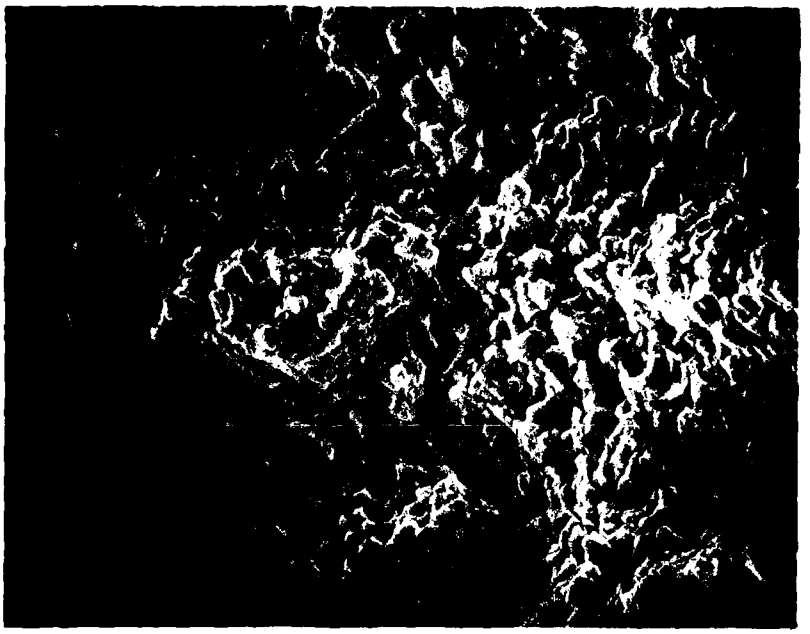

(a) Center of Specimen (1,000×)

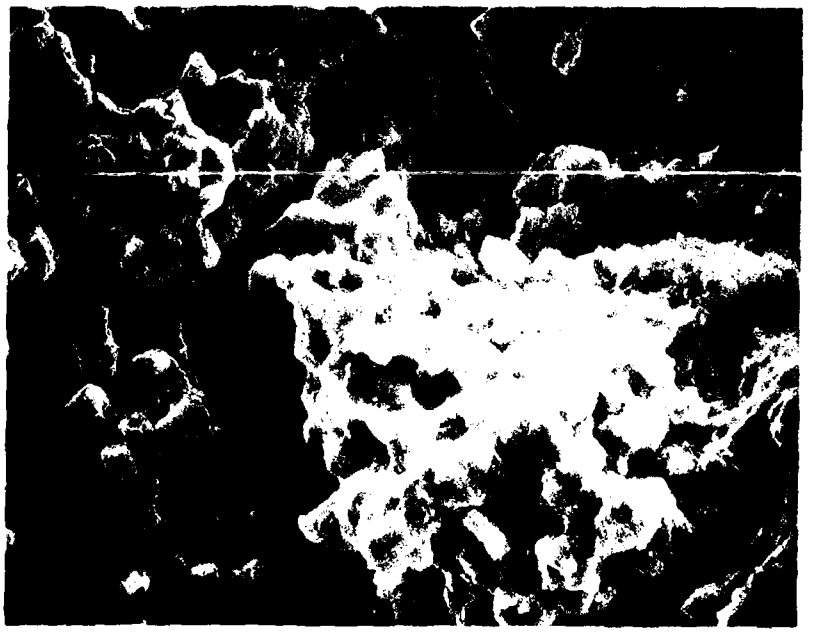

(b) Edge of Specimen (2,000×)

Figure 16. Micrographs of Fracture Surface of IN 100 (Gatorized) Formed Under Constant Load

The fracture mode was found to be intergranular in nature. The secondary cracks which were observed on the fracture surfaces were found to be present throughout the fracture surface and extended in all directions. The presence of oxide layers was also detected on the fracture surfaces. The intergranular fracture observed in this investigation is characteristic of creep failure, and the occurrence of this failure in the present case is thought to be grain-boundary-oxidation induced. However, only a test of this material under controlled atmospheric conditions (say, in vacuum or inert gas) could be used to substantiate this hypothesis.

Specimen #15-1, which was overheated to 843°C (1500°F) exhibited a faster crack-growth rate than that observed in other specimens. To ascertain whether the change in crack-growth rate was the result of microstructural differences (caused by overheating), optical metallography of the specimens heat treated at 732°C (1350°F) and at 843°C (1550°F) for 15 hr. was performed and the results compared. The optical micrographs did not reveal any difference in microstructure of the material for the above two heat treatments.

## REFERENCES


1. Materials Evaluation, SRL Quarterly Progress Reports for the periods 15 April 1976 - 15 July 1976, 15 July 1976 - 15 October 1976, 15 October 1976 - 15 January 1977, 15 April 1977 - 15 July 1977, 15 July 1977 - 15 October 1977, 15 October 1977 - 15 January 1978, 15 April 1978 - 15 July 1978, 15 July 1978 - 15 October 1978, 15 October 1978 - 15 January 1979, Air Force Contract F33615-76-C-5191, Air Force Materials Laboratory, Wright-Patterson Air Force Base, OH (Prepared by Research Applications Division, Systems Research Laboratories, Inc., 2800 Indian Ripple Road, Dayton, OH 45440).

2. Materials Evaluation, SRL Interim Technical Report for periods 15 April 1976 - 15 April 1977 and 15 April 1977 - 15 April 1978, Air Force Contract F33615-76-C-5191, Air Force Materials Laboratory, Wright-Patterson Air Force Base, OH (Prepared by Research Applications Division, Systems Research Laboratories, Inc., 2800 Indian Ripple Road, Dayton, OH 45440).

3. T. J. Rudolphi, "An Integral-Equation Solution for a Bounded Elastic Body with an Edge Crack: Mode I Deformations," Air Force Materials Laboratory Technical Report AFML-TR-78-113 (Air Force Materials Laboratory, Wright-Patterson Air Force Base, OH, July 1978).

4. Instruction Manual M400 Computer Control System 400MT/WPAFB (U.S. Data Engineering, Inc., April 1978).

5. J. W. Phillips, A. F. Mak, and N. E. Ashbaugh, "Stress-Wave Detection of an Edge Crack in an Elastic Rod," Int. J. Solids and Structures 14, 141 (1978).

6. D. E. Macha, A. F. Grandt, Jr., and B. J. Wicks, "Effects of Gas Turbine Engine Load Spectrum Variables on Crack Propagation," Presented at the ASTM Symposium on the Effect of Load Spectrum Variables on Fatigue Crack Initiation and Propagation, San Francisco, CA, 1979.

7. S. J. Hudak, Jr., A. Saxena, R. J. Bucci, and R. C. Malcolm, "Development of Standard Methods of Testing and Analyzing Fatigue Crack Growth Rate Data," Air Force Materials Laboratory Technical Report AFML-TR-78-40 (Air Force Materials Laboratory, Wright-Patterson Air Force Base, OH, May 1978).

8. "ANSI/ASTM E 399-78, Standard Test Method for Plane-Strain Fracture Toughness of Metallic Materials," 1978 Annual Book of ASTM Standards (American Society for Testing and Materials, Philadelphia, PA, 1978).

9. "ASTM E 647-78T, Tentative Test Method for Constant-Load-Amplitude Fatigue Crack Growth Rates Above $10^{-8}$ m/cycle," 1978 Annual Book of ASTM Standards, (American Society for Testing and Materials, Philadelphia, PA, 1978).




*U.S.Government Printing Office: 1980 — 657-084/466